Simultaneous CRISPR/Cas9-mediated editing of cassava *eIF4E* isoforms *nCBP-1* and *nCBP-2* confers elevated resistance to cassava brown streak disease

1. Gomez, Michael A.[1,3] and Lin, Z. Daniel[2,3]
2. Moll, Theodore[2]
3. Luebbert, Collin[2]
4. Chauhan, Raj Deepika[2]
5. Vijayaraghavan, Anupama[2]
6. Kelley Renninger[2]
7. Beyene, Getu[2]
8. Taylor, Nigel J. [2]
9. Carrington, J. [2]
10. Staskawicz, B.[1]
11. Bart, R.[2]*

[1] University of California, Berkeley, CA United States of America
[2] Donald Danforth Plant Science Center, St. Louis MO, United States of America
[3] These authors contributed equally to this work.
* Corresponding author: rbart@danforthcenter.org

Word count: 6948/7000 max (Summary, Main text, Table & Figure Legends)

Keywords: CRISPR/Cas9, genome editing, eIF4E, potyvirus, cassava brown streak disease

Summary

Cassava brown streak disease (CBSD) is a major constraint on cassava yields in East and Central Africa and threatens production in West Africa. CBSD is caused by two species of positive sense RNA viruses belonging to the family *Potiviridae*, genus *Ipomovirus*: *Cassava brown streak virus* (CBSV) and *Ugandan cassava brown streak virus* (UCBSV). Diseases caused by the family *Potyviridae* require the interaction of viral genome-linked protein (VPg) and host eukaryotic translation initiation factor 4E (eIF4E) isoforms. Cassava encodes five eIF4E isoforms: eIF4E, eIF(iso)4E-1, eIF(iso)4E-2, novel cap-binding protein-1 (nCBP-1), and nCBP-2. Yeast two-hybrid analysis detected interactions between both CBSV and UCBSV VPg proteins and cassava nCBP-1 and nCBP-2. CRISPR/Cas9-mediated genome editing was employed to generate *eif4e, ncbp-1, ncbp-2,* and *ncbp-1/ncbp-2* mutants in cassava cultivar 60444. Challenge with CBSV showed that *ncbp-1/ncbp-2* mutants displayed delayed and attenuated CBSD aerial symptoms, as well as reduced severity and incidence of storage root necrosis. Suppressed disease symptoms were correlated with reduced virus titer in storage roots relative to wild-type controls. However, full resistance to CBSD was not achieved, suggesting that remaining functional eIF4E isoforms may be compensating for the targeted mutagenesis of

nCBP-1 and *nCBP-2*. Future studies will investigate the contribution of these other isoforms to development of CBSD.

Introduction

Cassava brown streak disease (CBSD) is a threat to food and economic security for smallholder farmers in sub-Saharan Africa. First reported in the 1930s in lowland and coastal East Africa, CBSD has since spread west to higher altitudes in Uganda, Kenya, Tanzania, Burundi, and the Democratic Republic of Congo (Adams *et al.*, 2013; Alicai *et al.*, 2007; Bigirimana *et al.*, 2011; Mbanzibwa *et al.*, 2011; Mulimbi *et al.*, 2012). The CBSD vector is the whitefly *Bemisia tabaci* which has a broad geographical distribution across sub-Saharan Africa (Legg *et al.*, 2014). CBSD symptoms include leaf chlorosis, brown streaks on stems, and necrosis of the storage roots. CBSD immunity, or complete non-infection of the cassava plant (*Manihot esculenta* Crantz), has not been observed within known farmer cultivars (Kaweesi *et al.*, 2014). Infection can occur in resistant cultivars such as Kaleso and Namikonga, but multiplication, movement, and disease symptoms are limited (Kaweesi *et al.*, 2014). Tolerant cultivars Nachinyaya and Kiroba can be infected and support virus movement and replication, but with intermediate symptoms, while susceptible cassava cultivars 60444 and Albert support high levels of virus concentration and develop severe CBSD symptoms (Hillocks *et al.*, 2001; Maruthi *et al.*, 2014; Masiga *et al.*, 2014; Ogwok *et al.*, 2015). Since symptoms may be subtle or develop only within the underground storage roots, CBSD may claim an entire crop without the farmer's knowledge until harvest (Legg *et al.*, 2015; Patil *et al.*, 2015). Necrotic lesions render the storage roots unfit for market and human consumption with losses of up to 70% root weight reported (Hillocks *et al.*, 2001). The International Institute of Tropical Agriculture (IITA) estimated that CBSD causes $175 million loss in East Africa each year (Michael, 2013).

The causative agents of CBSD, *Cassava brown streak virus* (CBSV) and *Ugandan cassava brown streak virus* (UCBSV), belong to the family *Potyviridae* (Genus: *Ipomovirus*) (Revers and García, 2015). These non-enveloped, flexuous, filamentous viruses contain a positive-sense, single-stranded RNA, with a 3'-poly(A) terminus (King *et al.*, 2012). CBSV recruits host cellular translation machinery to produce a polyprotein of 2902 amino acids that is proteolytically cleaved into 10 mature proteins (Mbanzibwa *et al.*, 2009). A viral genome-linked (VPg) protein is covalently linked to the 5' end of the viral genome and is required for infection by this pathogen (Robaglia and Caranta, 2006; Wang and Krishnaswamy, 2012).

Resistance to plant pathogens can be controlled either through dominant or recessive gene inheritance. Resistance genes encoding nucleotide-binding leucine-rich repeat receptors, which are dominant sources of extreme resistance against adapted pathogens in many pathosystems, have been cloned and characterized for potyviral diseases, but an overrepresentation in recessive resistance to potyviruses is well documented (de Ronde et al., 2014; Revers and Nicaise, 2014). Recessive resistance to potyviruses is typically associated with mutations in the eukaryotic translation initiation factor 4E (eIF4E) protein family (Bastet *et al.*, 2017; Robaglia and Caranta, 2006). Ethyl methanesulfonate- and transposon-mutagenesis screens in *Arabidopsis thaliana* for decreased susceptibility to Turnip Mosaic potyvirus (TuMV) identified *eIF(iso)4E* as a loss of susceptibility locus (Duprat *et al.*, 2002; Lellis *et al.*, 2002). More broadly, polymorphisms in eIF4E isoforms of pepper, tomato, lettuce, pea, and other crops confer resistance to numerous potyviruses (Robaglia and Caranta, 2006). The direct physical interaction between potyvirus VPg and specific host eIF4E isoforms is well supported through *in vitro* and *in vivo* binding assays (Kang *et al.*, 2005; Leonard *et al.*, 2000; Schaad *et al.*, 2000; Wittmann *et al.*, 1997; Yeam *et al.*, 2007). In most of these cases, amino acid substitutions within the interaction domains on either VPg or eIF4E isoforms abolished infection, highlighting the necessity of eIF4E isoform interaction.

The eIF4E protein family plays an essential role in the initiation of cap-dependent mRNA translation. eIF4E isoforms interact with the 5'-7mGpppN-cap of mRNA and subsequently recruit a complex of initiation factors for ribosomal translation. eIF4E and its different isoforms, eIF(iso)4E and novel cap-binding protein (nCBP), vary in degrees of functional redundancy and may have undergone neo- or subfunctionalization (Browning and Bailey-Serres, 2015). Little is known regarding nCBPs, in particular. Studies in *A. thaliana* have shown that nCBP exhibits weak cap-binding, similar to eIF(iso)4E, and increased levels in cap-binding complexes at early stages of cell growth (Kropiwnicka *et al.*, 2015, Bush *et al.*, 2009). However, the specialized function of nCBPs remains unknown. Potyviruses hijack the eIF4E protein family via their VPg for translation initiation, genome stability, and/or viral movement (Fig S1) (Contreras-Paredes *et al.*, 2013; Eskelin *et al.*, 2011; Gao *et al.*, 2004; Miras *et al.*, 2017; Zhang *et al.*, 2006). Transgenic approaches leveraging amino acid changes that abolish interaction with VPg or loss of the VPg-associated eIF4E protein have previously been implemented as a form of potyviral disease control (Cui and Wang, 2017; Piron *et al.,* 2010; Wang, 2015).

Targeted genome editing techniques have emerged as alternatives to classical plant breeding and transgenic methods (Belhaj *et al.*, 2015). The CRISPR (Clustered Regularly Interspaced Short Palindromic Repeats)/Cas9 (CRISPR associated protein 9) system has rapidly become a favored tool for biotechnology because of its simple design and easy construction of reagents. The Cas9 nuclease is recruited to a specific site within the genome via a guide RNA (gRNA) (Jinek *et al.*, 2012). Upon binding, Cas9 induces a double strand break (DSB) at the target site (Belhaj *et al.*, 2015). Repair of the DSB by error-prone non-homologous end joining (NHEJ) can generate insertion or deletion (INDEL) mutations that disrupt gene function by altering the reading frame and/or generate a premature stop codon (Britt, 1999; Gorbunova and Levy, 1999). We aimed to apply the CRISPR/Cas9 technology to knockout the VPg-associated cassava eIF4E isoform(s). This approach to engineering potyvirus resistance has been successfully demonstrated in *A. thaliana* and cucumber (Chandrasekaran *et al.*, 2016; Pyott *et al.*, 2016). Here, we show that targeted mutagenesis of specific cassava *eIF4E* isoforms *nCBP-1* and *nCBP-2* by the CRISPR/Cas9 system reduces levels of CBSD associated disease symptoms and CBSV accumulation in storage roots. Simultaneous disruption of both *nCBP* isoforms resulted in a larger decrease in disease symptoms than disruption of either isoform individually.

Results

Identification and sequence comparison of eIF4E isoforms in cassava varieties

To identify the eIF4E family protein(s), a BLAST search of the AM560-2 cassava cultivar genome (assembly version 6.1) was done via Phytozome using *A. thaliana* eIF4E family proteins as the queries (Bredeson *et al.*, 2016; Goodstein *et al.*, 2012). Five cassava proteins were found that phylogenetically branched with the eIF4E, eIF(iso)4E, and nCBP sub-groups (Fig 1A). Two of the cassava eIF4E family proteins joined within the eIF(iso)4E sub-group, and another two joined within the nCBP sub-group. This is in agreement with findings by Shi *et al.* (2017). Percent identity analysis further supported this grouping as the eIF(iso)4E- and nCBP-similar proteins had high amino acid identity (Fig 1B). Based upon this phylogenetic analysis, one *eIF4E*, two *eIF(iso)4E*, and two *nCBP* genes cassava genes were re-named according to their sub-groups, as described in Fig 1C.

nCBP-1 and nCBP-2 isoforms interact with CBSV and UCBSV VPg in yeast

To identify the interaction partner(s) for the CBSV and UCBSV VPgs, a yeast two-hybrid system was used to assess the VPg-eIF4E isoform interactions. The VPg proteins from CBSV Naliendele isolate TZ:Nal3-1:07 (CBSV-Nal) and UCBSV isolate UG:T04-42:04 (UCBSV-T04) were fused to the B42 activation domain and transformed into yeast strain EGY48. All five cap-binding proteins were fused to the LexA DNA-binding domain and transformed into VPg yeast lines. Likewise fused, TuMV VPg and *A. thaliana* eIF(iso)4E were transformed into yeast as a positive control, and empty vectors were transformed as negative controls. Five colonies from each transformation were plated on selective media supplemented with X-gal. In this assay, a blue color is indicative of protein-protein interaction dependent activity of the β-galactosidase reporter. Based upon high amino acid sequence identity within eIF4E-family subgroups, we hypothesized both members of a sub-group would interact with CBSV and UCBSV VPgs. Both nCBP-1 and nCBP-2 showed strong interactions with the VPgs, visually comparable to the positive control (Fig. 2). *nCBP-1* and *nCBP-2* were selected for CRISPR/Cas9-mediated editing to abolish the critical VPg-eIF4E family protein interaction.

Site-specific mutation of eIF4E isoforms by transgenic expression of sgRNA-guided Cas9

CRISPR/Cas9 was employed to generate mutant alleles of cassava *eIF4E* isoforms. Seven constructs were assembled to target various sites in *nCBP-1*, *nCBP-2,* and *eIF4E* (Table 1). *Agrobacterium* carrying these constructs were then used to transform friable embryogenic calli (FEC) derived from cassava cultivar 60444 (Fig. 3). Transgenic T0 plants were selected in tissue culture using the *npt*II selectable marker in order to recover plants in which the CRISPR/Cas9 reagents had been integrated into the plant genome. Multiple independent T0 transgenic plant lines were recovered for each construct (Table S1). Sites in each *nCBP* gene were targeted to disrupt restriction enzyme recognition sequences (Fig. S2). Restriction digestion done on a PCR product from T0 plants using restriction enzyme SmlI indicated successful mutagenesis of both *nCBP* genes (Fig. S2). Cassava is diploid, carrying two copies of each *nCBP* gene. Absence of the wild-type digested product indicates that both alleles were successfully mutagenized.

The range of mutations generated in each transgenic plant was analyzed by subcloning and sequence analysis, revealing an array of homozygous, bi-allelic, heterozygous, complex, and wild-type genotypes (Table S1). Bi-allelic mutations contained different mutations on the two alleles. Heterozygous plants carried one mutagenized allele and one wild-type allele. Plants were considered complex if they carried more than two sequence patterns, strongly suggesting chimerism (Odipio *et al.,* 2017; Zhang *et al.,* 2016). The genotypes of edited plants had Cas9-induced INDELs ranging from insertions of 1 to 16 bp and deletions as large as 127 bp (Table S1). Review of all genotyped plants revealed that 13/55 (24%) carried homozygous mutations, 31/55 (56%) carried bi-allelic mutations, 1/55 (2%) were heterozygous, 5/55 (10%) were complex, and another 5/55 (10%) were wild-type genotypes (Table 1). In total, 80% of plants contained either homozygous or bi-allelic mutations, and CRISPR/Cas9 activity was observed in 91% of the plants studied.

Sequence analysis of INDEL-induced frameshifts in *nCBP*s identifies unpredicted *ncbp-1* splice variants

Given the yeast two-hybrid interaction between the nCBPs and viral VPg proteins, we chose to test the effects of mutations in *nCBP-1* and *nCBP-2* individually, as well as both *nCBP*s in tandem, in CBSV and UCBSV disease trials in a greenhouse. Lines with homozygous mutations in exon 1 were prioritized (Fig. 3). The mutant lines chosen for these trials, *ncbp-1*, *ncbp-2*, *ncbp-1/2* #2, and *ncbp-1/2* #8, each had an INDEL at the 3' end of the first exon of each targeted gene (Fig. 4). The INDELs either directly resulted in a frameshift or disrupted the exon-intron junction so that an out of frame splice variant was predicted to be produced (Fig. S3). To further characterize these mutations, cDNA clone sequencing (clone-seq) was done (Fig. 3, 5). The homozygous *ncbp-1* allele from *ncbp-1/2* #2 was also analyzed for comparison. Of nine *ncbp-1* clones from *ncbp-1/2* #2, eight displayed the wild-type splicing pattern (referred to as type 1) with the A-insertion predicted from genomic DNA sequence results. This generates a frameshift. One splice variant (referred to as type 2) was also observed (Fig. 5). This alternative splice form results in an insertion of 35 nucleotides but does not shift the reading frame. Thus, this splice variant encodes a full protein with a 12 amino acid internal insertion. This splicing pattern was not observed in any wild-type *nCBP-1* clones, however, may occur at low frequency.

Clone-seq analysis of seven *ncbp-1* clones from mutant line *ncbp-1/2* #8 cDNA similarly found predicted INDELs. Two clones displayed the wild-type (type 1) splicing pattern and the predicted A-deletion that alters the reading frame. Four clones showed a sequence pattern that suggests a third splicing variant (type 3) at an upstream alternative splice site (Fig. 5) (Reddy *et al.,* 2007). Both observed cDNA sequence patterns are frameshifted.

***ncbp-1/ncbp-2* double mutants exhibited reduced UCBSV symptom incidence and slowed CBSV symptom onset**

CBSV has been described as being more virulent than UCBSV (Kaweesi *et al.*, 2014; Mohammed *et al.*, 2012; Ogwok *et al.*, 2015). Challenge with a stronger pathogen may mask subtle phenotypes that could be presented during challenge with the weaker pathogen. As such, three disease trials for each virus species were carried out. The *ncbp-1, ncbp-2, ncbp-1/2 #2, ncbp-1/2* #8, and wild-type 60444 plants were chip-bud graft inoculated with either CBSV-Nal or UCBSV-T04 (Wagaba et. al, 2013). Aerial disease incidence was scored every week for 12 to 14 weeks after grafting. This analysis describes the percentage of plants showing any level of foliar or stem symptoms at each time point. At least five replicate plant clones were included for each genotype (n≥5). Inoculation with UCBSV-T04 did not produce stem symptoms. Consequently, only foliar disease incidence was recorded for those trials. Fluctuations in the percentage of plants that exhibited symptoms at each time point (% incidence) results from the shedding of symptomatic leaves throughout the experiment. Disease incidence for each genotype varied across experimental replicates, possibly due to variance in viral load of the chip-bud donor or a change in environmental conditions affecting disease pressure. However, a consistent relationship between genotypes was observed. Across all three experimental replicates, *ncbp-1/ncbp-2* double mutants exhibited reduced symptom incidence relative to wild-type plants and *ncbp-1*. The *ncbp-2* phenotype was intermediate between the double mutant and wild-type incidence rates (Fig. 6b, S4). Aerial UCBSV virus titer was measured for one experiment, but proved to be highly variable across biological replicates (Fig. S9).

In challenges with CBSV-Nal, wild-type plants produced strong foliar and stem symptoms in contrast to the UCBSV trials. Across all three experimental replicates, *ncbp-1/ncbp-2* double mutants exhibited delayed symptom development relative to wild type and *ncbp-1* (Fig. 6a, S4). In two experiments the double mutant lines reached 100% incidence at a markedly reduced rate relative to wild type and *ncbp-1*; in the remaining experiment, the same lines never rose above 43% incidence. *ncbp-2* exhibited symptom incidence development similar to wild type and *ncbp-1* in two experiments and displayed an intermediate phenotype in the third experiment (Fig 6b, S4a, S4b).

ncbp-1/ncbp-2 lines exhibit reduced aerial symptom severity after challenge with CBSV

For the described CBSV challenges, combined leaf-stem scores were also used to track aggregate aerial CBSD severity for each genotype over time (Table 2, Fig. 6c, S5). Wild-type, *ncbp-1*, and *ncbp-2* plants displayed similar levels of disease, although in one of three experiments *ncbp-2* developed statistically significantly less severe symptoms than wild type or *ncbp-1* (Fig. S5a). This experiment was the same one in which *ncbp-2* symptom incidence was intermediate between wild type/*ncbp-1* and *ncbp* double mutant levels (Fig. S4c). The *ncbp-1*/*ncbp-2* double mutants had greatly reduced CBSD severity in all three trials. Area under the disease progression curve (AUDPC) analysis revealed the reduced aerial symptom severity in *ncbp-1*/*ncbp-2* double mutants to be statistically significant in all three experimental replicates (Fig. 6d, S5). While *ncbp-1*/*ncbp-2* stem symptom severity was reduced in all three experiments, average leaf symptom severity tracked closely with wild type in one experiment (Fig. 7, S6, S7). Despite this, it is clear that mutating both *nCBP* isoforms had an effect on CBSD disease development.

ncbp-1/*ncbp-2* double mutant storage roots are less symptomatic and accumulate less virus

At 12 to 14 weeks after graft inoculation, storage roots were excavated and assessed for root necrosis. Only inoculation with CBSV-Nal produced storage root symptoms. Each storage root of a plant was divided into five sections and each section scored on a 1-5 scale for CBSD symptom severity (Fig. 8a). Average symptom scores for each genotype were compared. *ncbp-2* and *ncbp-1*/*ncbp-2* mutant lines all exhibited significantly reduced symptom scores relative to wild type and *ncbp-1* (Fig. 8b). Reverse transcription-quantitative polymerase chain reaction (qPCR) was used to measure CBSV-Nal RNA levels in *ncbp-1*/*ncbp-2* double mutants. Viral RNA levels in *ncbp-1*/*ncbp-2* roots were reduced 43-45% compared to wild-type roots (Fig. 8c).

Discussion

The CRISPR/Cas9 system has emerged as a powerful tool for plant genome editing and rapid crop improvement. In the context of disease resistance in crop species, this system has been employed to target *mildew-resistance locus O* (*MLO*) in wheat, and generate broad potyvirus resistance in cucumber by disrupting function of the e*IF4E* gene (Chandrasekaran *et al.*, 2016; Wang *et al.*, 2014). In the present study, we targeted the *nCBP*s to assess their putative function as CBSD susceptibility factors in cassava.

Previous studies have shown that host eIF4E and viral VPg interaction is necessary for potyviral infection (Ashby *et al.*, 2011; Charron *et al.*, 2008; Kang *et al.*, 2005; Leonard *et al.*, 2000; Yeam *et al.*, 2007). We identified five eIF4E family members in cassava, corroborating a recent analysis by Shi *et al.* (2017). Cassava is thought to be an ancestral allopolyploid, likely yielding the two *eIF(iso)4E* and *nCBP* genes (Fregene *et al.*, 1997). The presence of multiple eIF4E isoforms may indicate sub-functionalization and specialization in translational control of differently methylated mRNA cap structures, or confer some functional redundancy that eases constraints on eIF4E evolution for potyvirus resistance (Carberry *et al.*, 1991; Charron *et al.*, 2008; Moury *et al.*, 2014). Attempts to identify markers associated with CBSD resistance indicate that multiple loci are involved, and transcriptional analyses suggest the contribution of hormone signaling pathways (Maruthi *et al.*, 2014; Masumba *et al.*, 2017). Examination of CBSD-resistant, -tolerant, and -susceptible cultivars by Shi and colleagues also found that these categories are not associated with *eIF4E* family single nucleotide polymorphisms (Shi *et al.*, 2017). As such, a biochemical study of the VPg and eIF4E family interaction was essential to identify a potential susceptibility gene(s).

Yeast two-hybrid analysis showed strong interactions between the nCBPs and the CBSV-Naliendele and UCBSV-T04 VPg proteins, to levels visually equivalent to the positive control TuMV VPg-*A. thaliana* eIF(iso)4E interaction (Fig. 2). First identified in *A. thaliana*, nCBP has a distinct amino acid sequence and exhibits methylated-cap-binding property (Kropiwnicka *et al.*, 2015; Ruud *et al.*, 1998). To date, there is no precedent for recruitment of nCBPs by VPg proteins belonging to the family *Potyviridae*. However, this isoform has been identified as a novel recessive resistance gene toward viruses in the *Alphaflexiviridae* and *Betaflexiviridae* families (Keima *et al.*, 2017). In the case of potexvirus *Plantago asiatica mosaic virus* (PlAMV), nCBP loss in *A. thaliana* impaired viral cell-to-cell movement by inhibiting accumulation of viral movement proteins from a subgenomic RNA. It is unclear if *A. thaliana* nCBP is either required for subgenomic RNA stability or translation of PlAMV movement proteins. In contrast, there is evidence that many members of *Potyviridae* produce the potyvirus P3N-PIPO movement protein through RNA polymerase slippage (Hagiwara-Komoda *et al.*, 2016; Olspert *et al.*, 2015; Rodamilans *et al.*, 2015). As such, while nCBP may similarly play a critical role in the accumulation of the CBSV movement protein, the underlying mechanism is likely to be different from those used during *Alpha-* and *Betaflexavirdae* infection. It has also been found that distantly related potyviruses that infect a common host may utilize different eIF4E isoforms for movement (Contreras-Paredes *et al.*, 2013; Eskelin *et al.*, 2011; Gao *et al.*, 2004; Miras *et al.*, 2017). Furthermore, evidence suggests that some potyviruses may utilize one specific isoform for translation and another distinct isoform for movement (Contreras-Paredes *et al.*, 2013; Gao *et al.*, 2004). This complexity makes it difficult to predict what roles cassava nCBPs may have in the CBSV life cycle. Further study is required to characterize the role of nCBP in translation, genome stability, and viral movement processes.

Five CRISPR/Cas9 expression constructs were designed and transgenically integrated into the cassava genome to target the *nCBP* genes individually and simultaneously. In transgenic plant lines, mutations were detected by restriction enzyme site loss analysis and Sanger sequencing. We observed homozygous, bi-allelic, heterozygous, complex, and wild-type genotypes. Homozygous mutations may have been generated by identical NHEJ repair, or homologous recombination-based repair from the opposite allele. Considering the low incidence of the latter in plants, identical NHEJ repair may be more likely (Peng *et al.*, 2016). While transgenic plants derived from FECs are thought to be of single cell origin (Fig. 3a), reducing the likelihood of transgenic chimeras (Schreuder *et al.*, 2001; Taylor *et al.*, 1996), Odipo et al. (2017) have reported the production of chimeric plants via CRISPR/Cas9-mediated gene editing of phytoene desaturase in cassava. In depth analyses of lines with complex genotypes were not pursued, but they are likely chimeras resulting from Cas9/sgRNA activity being delayed until after embryogenic units began to replicate (Odipio *et al.,* 2017; Zhang *et al.,* 2014). Integrating CRISPR/Cas9 constructs into the cassava genome proved to be efficient for achieving gene editing as 91% of the transformed plant lines carried INDELs at the target sites, and desired homozygous and bi-allelic mutations were observed in 80% of plant lines. These frequencies compare favorably to previous CRISPR/Cas9-mediated mutagenesis studies in cassava, rice and tomato (Ma *et al.*, 2015; Odipio *et al.*, 2017; Pan *et al.*, 2016). Homozygous and bi-allelic genotype frequencies in rice and tomato were approximately 80% and 19%, respectively.

CBSD inoculation experiments were limited to plant lines carrying homozygous and bi-allelic mutations that resulted in a frameshift or disrupted the exon-intron junction, thus resulting in the production of frameshifted splice variants. Single-*nCBP* and double-*nCBP* mutant lines were challenged with isolates CBSV-Naliendele and UCBSV-T04 (Beyene *et al.*, 2017; Wagaba *et al.*, 2013). Levels of resistance to CBSD were strongly correlated with disrupting function of both *nCBP* genes. Over the course of 12 to 14 weeks, double-*nCBP* mutant lines exhibited delayed CBSD aerial (combined leaf and stem) symptom onset and reduced severity. Full resistance to CBSD was not achieved as some brown streaking of the stem occurred in double mutants, and leaf symptom severity tracked closely with wild type in our last experiment. Furthermore, toward the end of each challenge, aerial symptom incidence in the double-*nCBP* mutants approached wild-type levels (Fig. 6, Fig. S4). Single-*nCBP* mutants were generally not significantly different from the susceptible wild-type plants in response to CBSV-Nal challenges, but symptom incidence for *ncbp-2* fluctuated between wild-type and double mutant levels across UCBSV-T04 challenges. These results could be due to UCBSV being less virulent than CBSV (Kaweesi *et al.*, 2014; Mohammed *et al.*, 2012; Ogwok *et al.*, 2015). nCBP-2 may be more important for viral accumulation, and it could be that the mutant phenotype is masked by challenge with a more virulent pathogen or conditions conducive to high disease pressure. The latter may also influence inoculum concentrations in donor plants and result in the observed experiment-to-experiment variation in disease severity (Fig. S4, S5, S6, S7). This is consistent with observations that increases in *ncbp-2* symptom incidence to wild-type levels occurred when symptom incidence in *ncbp-1/ncbp-2* plants was elevated relative to other experiments. Variation in disease pressure may also explain the inconsistent leaf phenotype in the double-*nCBP* mutant plants. The mechanisms underlying CBSD leaf and stem symptom development are unknown and it is possible that symptoms in different tissue types can be unequally influenced by varying levels of disease pressure.

At our challenge endpoints, symptom development and virus accumulation in the agronomically important tuberous roots were analyzed. Consistent with observations of aerial tissues, symptom severity in the roots was significantly lower in the double-*nCBP* mutants than in wild-type plants. CBSV titers in roots were significantly reduced in the double-*nCBP* mutants. Interestingly, the mutagenesis of *nCBP-2* resulted in reduced symptom severity as compared to wild-type plants and *ncbp-1* mutant lines. This result may be explained by the 10 fold higher expression of *nCBP-2* in the roots, but also highlights the possibility that nCBP-1 and nCBP-2 are not fully redundant (Fig. S8) (Wilson *et al.*, 2017). Assuming that the effects of *nCBP* mutations are due to the disruption of VPg-nCBP interactions, it is also possible that CBSV VPg may have a higher dependence for nCBP-2 than nCBP-1. Forcing CBSV to utilize less abundant isoforms, or those with suboptimal binding affinities, could attenuate CBSD progression. Additional transcriptional and biochemical studies will be needed to investigate these hypotheses.

Several explanations may account for the incomplete CBSD resistance of double-*nCBP* mutant cassava plants. First, unpredicted splice variants may have coded for proteins that were biologically functional for viral infection, at least in part (Fig. 5). The activation of normally silent, cryptic, splice sites is consistent with the intron definition of splicing (Lal *et al.*, 1999). Under this model, disruption of the wild-type splice site motifs, typically dinucleotides GU and AG at the 5' and 3' termini of introns, respectively, can activate cryptic splice sites that redefine intron boundaries and consequently frameshifts the mature transcript (Reddy et al., 2007). This is consistent with our cDNA clone-seq analysis identifying a type 3 splice variant of *ncbp-1* from line *ncbp-1/2* #8. However, the type 2 *ncbp-1* variant of *ncbp-1/2* #2 does not appear to be the result of splice site disruptions. Furthermore, it codes for full length nCBP-1 with a 12 amino acid extension. It is possible that similar unpredicted splice variants exist at low abundance in *ncbp-1/*2 #8. Complementation assays will need to be performed to determine whether such putative splice variants can be utilized by the viruses. The level of these transcripts and/or their encoded protein's affinity for CBSV and UCBSV VPgs are likely low considering the the clear impact on CBSD development. Second, CBSV and UCBSV VPgs may have some inherent, low-level affinity for the other eIF4E isoforms. Co-expression of the cassava eIF(iso)4E-1 and -2 with VPg from both species showed weak reporter activation that could be interpreted as weak interaction or reporter auto-activation as seen in the TuMV VPg plus empty vector control (Fig. 2). VPg is an intrinsically disordered protein, which could enable it to bind several different proteins (Jiang and Laliberté, 2011). The ability to use multiple eIF4E isoforms has precedence, such as in *Pepper veinal mottle potyvirus* for which simultaneous mutations of both eIF4E and eIF(iso)4E is required to restrict infection (Gauffier *et al.*, 2016; Ruffel *et al.*, 2006). Recruitment of eIF4E or the two eIF(iso)4E isoforms by CBSV/UCBSV could result in sub-optimal viral replication or movement, resulting in lower symptom severity and incidence. This has previously been hypothesized by Chandrasekaran et al. (2016) for breaking of *eif4e*-mediated resistance in cucumber. Further investigation will be required to test this hypothesis in cassava.

CBSD remains a major threat to food security in sub-Saharan Africa. Mitigation of crop losses is imperative to sustaining Africa's rapidly growing population. Due to the challenges of breeding cassava, genetic editing strategies provide an attractive means to engineer disease resistance. In this study, we show that simultaneous CRISPR/Cas9-mediated editing of the *nCBP-1* and *nCBP-2* genes confers statistically significantly elevated resistance to CBSD. Editing of these host translation factors significantly hampers CBSV accumulation in the plant. By stacking this approach with other forms of resistance such as RNAi, potential exists to provide improved cassava varieties with robust and durable resistance to CBSD.

Materials and Methods

Production of plants and growth conditions

Transgenic cassava lines of cultivar 60444 were generated and maintained *in vitro* as described previously (Taylor *et al.*, 2012). *In vitro* plantlets were propagated, established in soil, and transferred to the greenhouse (Taylor *et al.*, 2012; Wagaba *et al.*, 2013). Throughout the course of a disease trial, all plants were treated bi-weekly for pest control by gently spraying the undersides of all leaves with water.

Identification and phylogenetic analysis of eIF4E isoforms

BLAST search of the AM560-2 cassava cultivar genome was done via Phytozome V10 using *A. thaliana* eIF4E family proteins as the queries. The coding sequences of each isoform were verified by comparison to RNA-seq data (Cohn *et al.*, 2014). Clustal Omega (EMBL-EBI) was used to generate the percent identity matrix of all eIF4E isoform amino acid sequences (Goujon *et al.*, 2010; Sievers *et al.*, 2014). MEGA 6 software was used to generate a phylogenetic tree of the cassava and *A. thaliana* eIF4E isoforms (Tamura *et al*., 2013). The evolutionary history was inferred by using the Maximum Likelihood method based on the Le_Gascuel_2008 model (Le and Gascuel, 1993). This amino acid substitution model was determined as best fit using the MEGA 6 model test. The tree with the highest log likelihood (-2025.7966) is shown. Initial tree(s) for the heuristic search were obtained automatically by applying Neighbor-Join and BioNJ algorithms to a matrix of pairwise distances estimated using a JTT model, and then selecting the topology with superior log likelihood value. A discrete Gamma distribution was used to model evolutionary rate differences among sites (5 categories (+*G*, parameter = 1.9218)). The analysis involved 9 amino acid sequences. All positions containing gaps and missing data were eliminated.

CRISPR/Cas9 binary construct design

CRISPR/Cas9 construct design and assembly of entry clone pCR3 were conducted as described by Paula de Toledo Thomazella *et al.* (2016). CRISPR/Cas9 constructs targeting two sites were assembled via Gibson Assembly of the other U6-26/gRNA into the *Sac*II site of the entry clone. Flanked by the attL1 and attL2 recombination sequences, the cassette carrying the Cas9/gRNA expression system was Gateway cloned into the binary destination vector pCAMBIA2300 (Hajdukiewicz *et al.*, 1994).

gRNA design and cloning

Target sequences were identified in *nCBP-1* and *nCBP-2* genes of cassava using the online CRISPR-P software (Lei *et al.*, 2014). This tool was used to select targets with predicted cut sites within exons, minimal off-target potential, and overlapping restriction enzyme recognition sites.

gRNA forward and reverse primers were designed with overhangs compatible with the BsaI-site described above. The Golden Gate (GG) cloning method was used to BsaI digest the pCR3 vector and ligate in the gRNA. In the case of the dual targeting CRISPR/Cas9 construct, the pCR3 vector bearing gRNA1 was digested with SacII, a site within the LR clonase attL sequences. The *A*. *thaliana* U6-26 promoter and gRNA2 were PCR amplified using primers suitable for Gibson Assembly into the SacII cut site of the digested pCR3-gRNA1 vector. For Gibson Assembly, 100 ng of SacII-digested vector was incubated with 200 ng of U6-26p-gRNA2 PCR amplicon and Gibson Assembly Master Mix for one hour and transformed into *E. coli* (NEB5a). Sequences of cloned CRISPR constructs were verified via Sanger sequencing.

Yeast two-hybrid

The *eIF4E* isoforms were amplified by PCR using primers suitable for Gibson Assembly into the *BamHI* site of pEG202. Yeast codon optimized coding sequences of the CBSV and UCBSV VPg were synthesized through Genewiz, Inc (South Plainfield, NJ, USA). The VPg coding sequences were amplified using primers suitable for Gibson Assembly into the *EcoRI* site of pEG201. Yeast two-hybrid analyses were carried out as described previously (Kim *et al.*, 2014).

Genotyping and mutant verification

100 mg of leaf tissue was collected from T0 transgenic cassava *in vitro* plantlets and genomic DNA extracted using the CTAB extraction procedure (Murray and Thompson, 1980). Transgenic plants were genotyped for Cas9-induced mutagenesis via restriction enzyme site loss (RESL) and Sanger sequencing (Voytas, 2013). Initially, 100 ng of genomic DNA was PCR amplified

using primers encompassing the Cas9 target sites. PCR amplicons were gel purified on 1.5% agarose gel and purified with the QIAquick Gel Extraction Kit. For RESL analysis, 50 ng of PCR amplicon were digested with restriction enzyme SmlI for 12 hours, then run and visualized on a 1.5% agarose gel. For genomic and cDNA sequence analysis, the amplicons were subcloned and Sanger sequenced through the UC Berkeley DNA Sequencing Facility. Between six to eight clones were sequenced to discriminate INDEL polymorphisms and sequences were aligned to the intact *nCBP-1* and *nCBP-2* using SnapGene software (from GSL Biotech; available at snapgene.com).

CBSV and UCBSV inoculation and disease scoring

Prior to virus challenge, micropropagated cassava plantlets were transplanted to soil, allowed to acclimate for six to eight weeks, and chip-bud graft inoculation performed as described previously (Wagaba *et al.*, 2013). Briefly, one plant of each genotype received an axillary bud from a single previously infected wild type plant, resulting in one inoculation cohort. Multiple cohorts were used in a single experiment to control for donor plants with varying viral concentrations.

Shoot tissues were scored two to three times a week for 12 to 14 weeks. Leaves and stems were each scored on separate 0-4 scales (Table 2). Leaf and stem scores were then summed to generate an overall aerial severity score for a particular time point. These data were used to calculate the area under the disease progression curve (Simko and Piepho, 2012). To assess symptom severity in storage roots, each storage root was evenly divided into five pieces along its length. Each storage root piece was then sectioned into one-centimeter slices and the maximum observed severity was used to assign a symptom severity score to that storage root piece. The scores for all storage root pieces of a given plant were then averaged to determine the overall severity score.

Storage root viral titer quantification

Five to ten representative storage root slices per plant were collected for viral titer quantification. Samples were flash frozen in liquid nitrogen and lyophilized for two days. Lyophilized storage roots were pulverized in 50 mL conical tubes with a FastPrepTM-24 instrument (MP Biomedicals) and 75 mg of pulverized tissue was aliquoted into Safe-Lock microcentrifuge tubes (Eppendorf) pre-loaded with two mm zirconia beads (BioSpec Products). Samples were flash frozen in liquid nitrogen, further homogenized to a finer consistency, and one mL of Fruit-mate (Takara) added to each sample. Samples were homogenized and subsequently centrifuged to remove debris. The supernatant was removed, mixed with an equal volume of TRIzol LS (Thermo Fisher), and the resulting mixture processed with the Direct-zol RNA MiniPrep kit (Zymo Research). Resulting total RNA was normalized to a standard concentration and used for cDNA synthesis with SuperScript III reverse transcriptase (Thermo Fisher).

Quantitative PCR was done with SYBR Select Master Mix (Thermo Fisher) on a CFX384 Touch Real-Time PCR Detection System (Bio-Rad). Primers specific for CBSV-Nal *HAM1-LIKE* and cassava *PP2A4* were used for relative quantitation (Table S2). Normalized relative quantities were calculated using formulas described by Hellemans *et al.* (2007). For combined analysis of all experimental replicates, normalized relative quantities for all samples were further normalized as a ratio to the geomean of wild type for their respective experiments. Data were then pooled and a Mann-Whitney U test was used to assess statistical differences.

Acknowledgments

We are grateful for valuable advice and discussion with members of the VIRCA group. We thank Claire Albin, Maxwell Braud, the Staskawicz lab staff, the DDPSC tissue culture facility, and the DDPSC greenhouse staff for their work supporting this study. Funding in the Staskawicz Laboratory was provided by the Two Blades Foundation. Funding to R.B. and J.C. from the Bill and Melinda Gates Foundation (OPP1125410). The authors declare no conflicts of interest.

References

Adams, I.P., Abidrabo, P., Miano, D.W., et al. (2013) High throughput real-time RT-PCR assays for specific detection of cassava brown streak disease causal viruses, and their application to testing of planting material. *Plant Pathol.* **62**, 233–242.

Alicai, T., Omongo, C.A., Maruthi, M.N., Hillocks, R.J., Baguma, Y., Kawuki, R., Bua, A., Otim-Nape, G.W. and Colvin, J. (2007) Re-emergence of Cassava Brown Streak Disease in Uganda. *Plant Dis.* **91**, 24–29.

Ashby, J.A., Stevenson, C.E.M., Jarvis, G.E., Lawson, D.M. and Maule, A.J. (2011) Structure-Based Mutational Analysis of eIF4E in Relation to sbm1 Resistance to Pea Seed-Borne Mosaic Virus in Pea Bendahmane, M., ed. *PLoS One* **6**, e15873.

Bastet, A., Robaglia, C. and Gallois, J.-L. (2017) eIF4E Resistance: Natural Variation Should Guide Gene Editing. *Trends Plant Sci.* **22**, 411–419.

Belhaj, K., Chaparro-Garcia, A., Kamoun, S., Patron, N.J. and Nekrasov, V. (2015) Editing plant genomes with CRISPR/Cas9. *Curr. Opin. Biotechnol.* **32**, 76–84.

Beyene, G., Chauhan, R.D., Ilyas, M., Wagaba, H., Fauquet, C.M., Miano, D., Alicai, T. and Taylor, N.J. (2017) A Virus-Derived Stacked RNAi Construct Confers Robust Resistance to Cassava Brown Streak Disease. *Front. Plant Sci.* **7**, 2052.

Bigirimana, S., Barumbanze, P., Ndayihanzamaso, P., Shirima, R. and Legg, J.P. (2011) First report of cassava brown streak disease and associated *Ugandan cassava brown streak virus* in Burundi. *New Dis. Reports* **24**, 26.

Bredeson, J. V, Lyons, J.B., Prochnik, S.E., et al. (2016) Sequencing wild and cultivated cassava and related species reveals extensive interspecific hybridization and genetic diversity. *Nat. Biotechnol.* **34**, 562–570.

Britt, A.B. (1999) Molecular genetics of DNA repair in higher plants. *Trends Plant Sci.* **4**, 20–25.

Browning, K.S. and Bailey-Serres, J. (2015) Mechanism of Cytoplasmic mRNA Translation.

Arab. B. **13**, e0176.

Bush, M.S., Hutchins, A.P., Jones, A.M.E., Naldrett, M.J., Jarmolowski, A., Lloyd, C.W. and Doonan, J.H. (2009) Selective recruitment of proteins to 5′ cap complexes during the growth cycle in Arabidopsis. Plant J. 59, 400–412.

Carberry, S.E., Goss, D.J. and Darzynkiewicz, E. (1991) A comparison of the binding of methylated cap analogs to wheat germ protein synthesis initiation factors 4F and (iso) 4F. *Biochemistry* **30**, 1624–1627.

Chandrasekaran, J., Brumin, M., Wolf, D., Leibman, D., Klap, C., Pearlsman, M., Sherman, A., Arazi, T. and Gal-On, A. (2016) Development of broad virus resistance in non-transgenic cucumber using CRISPR/Cas9 technology. *Mol. Plant Pathol.* **17**, 1140–1153.

Charron, C., Nicolaï, M., Gallois, J.-L., Robaglia, C., Moury, B., Palloix, A. and Caranta, C. (2008) Natural variation and functional analyses provide evidence for co-evolution between plant eIF4E and potyviral VPg. *Plant J.* **54**, 56–68.

Cohn, M., Bart, R.S., Shybut, M., et al. (2014) Xanthomonas axonopodis Virulence Is Promoted by a Transcription Activator-Like Effector–Mediated Induction of a SWEET Sugar Transporter in Cassava. *Mol. Plant-Microbe Interact. MPMI* **27**, 1186–1198.

Contreras-Paredes, C.A., Silva-Rosales, L., Daròs, J.-A., Alejandri-Ramírez, N.D. and Dinkova, T.D. (2013) The absence of eukaryotic initiation factor eIF(iso)4E affects the systemic spread of a Tobacco etch virus isolate in Arabidopsis thaliana. *Mol. Plant-Microbe Interact. MPMI* **26**, 461–70.

Cui, H. and Wang, A. (2017) An efficient viral vector for functional genomic studies of Prunus fruit trees and its induced resistance to Plum pox virus via silencing of a host factor gene. Plant Biotechnol. J. 15, 344–356.

Duprat, A., Caranta, C., Revers, F., Menand, B., Browning, K.S. and Robaglia, C. (2002) The Arabidopsis eukaryotic initiation factor (iso)4E is dispensable for plant growth but required for susceptibility to potyviruses. *Plant J.* **32**, 927–934.

Eskelin, K., Hafrén, A., Rantalainen, K.I. and Mäkinen, K. (2011) Potyviral VPg enhances viral RNA Translation and inhibits reporter mRNA translation in planta. *J. Virol.* **85**, 9210–21.

Fregene, M., Angel, F., Gomez, R., Rodriguez, F., Chavarriaga, P., Roca, W., Tohme, J. and Bonierbale, M. (1997) A molecular genetic map of cassava (Manihot esculenta Crantz). *TAG Theor. Appl. Genet.* **95**, 431–441.

Gao, Z., Johansen, E., Eyers, S., Thomas, C.L., Noel Ellis, T.H. and Maule, A.J. (2004) The potyvirus recessive resistance gene, sbm1, identifies a novel role for translation initiation factor eIF4E in cell-to-cell trafficking. *Plant J.* **40**, 376–385.

Gauffier, C., Lebaron, C., Moretti, A., Constant, C., Moquet, F., Bonnet, G., Caranta, C. and Gallois, J.-L. (2016) A TILLING approach to generate broad-spectrum resistance to potyviruses in tomato is hampered by *eIF4E* gene redundancy. *Plant J.* **85**, 717–729.

Goodstein, D.M., Shu, S., Howson, R., et al. (2012) Phytozome: a comparative platform for green plant genomics. *Nucleic Acids Res.* **40**, D1178–D1186.

Gorbunova, V. and Levy, A.A. (1999) How plants make ends meet: DNA double-strand break repair. *Trends Plant Sci.* **4**, 263–269.

Goujon, M., McWilliam, H., Li, W., Valentin, F., Squizzato, S., Paern, J. and Lopez, R. (2010) A new bioinformatics analysis tools framework at EMBL-EBI. *Nucleic Acids Res.* **38**, W695–W699.

Hagiwara-Komoda, Y., Choi, S.H., Sato, M., et al. (2016) Truncated yet functional viral protein produced via RNA polymerase slippage implies underestimated coding capacity of RNA viruses. *Sci. Rep.* **6**, 21411.

Hajdukiewicz, P., Svab, Z. and Maliga, P. (1994) The small, versatile pPZP family of Agrobacterium binary vectors for plant transformation. *Plant Mol. Biol.* **25**, 989–994.

Hellemans, J., Mortier, G., Paepe, A. De, Speleman, F. and Vandesompele, J. (2007) qBase relative quantification framework and software for management and automated analysis of real-time quantitative PCR data. *Genome Biol.* **8**, R19.

Hillocks, R.J., Raya, M.D., Mtunda, K. and Kiozia, H. (2001) Effects of Brown Streak Virus Disease on Yield and Quality of Cassava in Tanzania. *J. Phytopathol.* **149**, 389–394.

Jiang, J. and Laliberté, J.-F. (2011) The genome-linked protein VPg of plant viruses—a protein with many partners. *Curr. Opin. Virol.* **1**, 347–354.

Jinek, M., Chylinski, K., Fonfara, I., Hauer, M., Doudna, J.A. and Charpentier, E. (2012) A programmable dual-RNA-guided DNA endonuclease in adaptive bacterial immunity. *Science* **337**, 816–21.

Kang, B.-C., Yeam, I., Frantz, J.D., Murphy, J.F. and Jahn, M.M. (2005) The pvr1 locus in Capsicum encodes a translation initiation factor eIF4E that interacts with Tobacco etch virus VPg. *Plant J.* **42**, 392–405.

Kaweesi, T., Kawuki, R., Kyaligonza, V., Baguma, Y., Tusiime, G. and Ferguson, M.E. (2014) Field evaluation of selected cassava genotypes for cassava brown streak disease based on symptom expression and virus load. *Virol. J.* **11**, 216.

Keima, T., Hagiwara-Komoda, Y., Hashimoto, M., Neriya, Y., Koinuma, H., Iwabuchi, N., Nishida, S., Yamaji, Y. and Namba, S. (2017) Deficiency of the eIF4E isoform nCBP limits the cell-to-cell movement of a plant virus encoding triple-gene-block proteins in Arabidopsis thaliana. *Sci. Rep.* **7**, 39678.

Kim, J., Kang, W.-H., Hwang, J., Yang, H.-B., Dosun, K., Oh, C.-S. and Kang, B.-C. (2014) Transgenic *Brassica rapa* plants over-expressing eIF(iso)4E variants show broad-spectrum *Turnip mosaic virus* (TuMV) resistance. *Mol. Plant Pathol.* **15**, 615–626.

King, A.M.Q., Adams, M.J., Carsten, E.B. and Lefkowitz, E.J. (2012) Virus Taxonomy: Classification and Nomenclature of Viruses. Ninth Report of the International Committee on Taxonomy of Viruses., Elsevier.

Kropiwnicka, A., Kuchta, K., Lukaszewicz, M., Kowalska, J., Jemielity, J., Ginalski, K., Darzynkiewicz, E. and Zuberek, J. (2015) Five eIF4E isoforms from Arabidopsis thaliana are characterized by distinct features of cap analogs binding. *Biochem. Biophys. Res. Commun.* **456**, 47–52.

Lal, S., Choi, J.H., Shaw, J.R. and Hannah, L.C. (1999) A splice site mutant of maize activates cryptic splice sites, elicits intron inclusion and exon exclusion, and permits branch point elucidation. *Plant Physiol.* **121**, 411–8.

Le, S.Q. and Gascuel, O. (2008) An Improved General Amino Acid Replacement Matrix. *Mol. Biol. Evol.* **25**, 1307–1320.

Legg, J.P., Kumar, P.L., Makeshkumar, T., Tripathi, L., Ferguson, M., Kanju, E., Ntawuruhunga, P. and Cuellar, W. (2015) Cassava Virus Diseases□: Biology, Epidemiology, and Management.

Legg, J.P., Shirima, R., Tajebe, L.S., Guastella, D., Boniface, S., Jeremiah, S., Nsami, E., Chikoti, P. and Rapisarda, C. (2014) Biology and management of Bemisia whitefly vectors of cassava virus pandemics in Africa. *Pest Manag. Sci.* **70**, 1446–1453.

Lei, Y., Lu, L., Liu, H.-Y., Li, S., Xing, F. and Chen, L.-L. (2014) CRISPR-P: A Web Tool for Synthetic Single-Guide RNA Design of CRISPR-System in Plants. *Mol. Plant* **7**, 1494–1496.

Lellis, A.D., Kasschau, K.D., Whitham, S.A. and Carrington, J.C. (2002) Loss-of-susceptibility mutants of Arabidopsis thaliana reveal an essential role for eIF(iso)4E during potyvirus infection. *Curr. Biol.* **12**, 1046–1051.

Leonard, S., Plante, D., Wittmann, S., et al. (2000) Complex Formation between Potyvirus VPg and Translation Eukaryotic Initiation Factor 4E Correlates with Virus Infectivity. *J. Virol.* **74**, 7730–7737.

Ma, X., Zhang, Q., Zhu, Q., et al. (2015) A Robust CRISPR/Cas9 System for Convenient, High-Efficiency Multiplex Genome Editing in Monocot and Dicot Plants. *Mol. Plant* **8**, 1274–1284.

Maruthi, M.N., Bouvaine, S., Tufan, H.A., Mohammed, I.U. and Hillocks, R.J. (2014) Transcriptional Response of Virus-Infected Cassava and Identification of Putative Sources of Resistance for Cassava Brown Streak Disease Fang, D.D., ed. *PLoS One* **9**, e96642.

Masiga, C.W., Mugoya, C., Ali, R., et al. (2014) Enhanced Utilization of Biotechnology Research and Development Innovations in Eastern and Central Africa for Agro-ecological Intensification. In Challenges and Opportunities for Agricultural Intensification of the Humid Highland Systems of Sub-Saharan Africa., pp. 97–104. Cham: Springer International Publishing.

Masumba, E.A., Kapinga, F., Mkamilo, G., et al. (2017) QTL associated with resistance to cassava brown streak and cassava mosaic diseases in a bi-parental cross of two Tanzanian farmer varieties, Namikonga and Albert. *Theor. Appl. Genet.*, 1–22.

Mbanzibwa, D.R., Tian, Y., Mukasa, S.B. and Valkonen, J.P.T. (2009) Cassava brown streak virus (Potyviridae) encodes a putative Maf/HAM1 pyrophosphatase implicated in reduction of mutations and a P1 proteinase that suppresses RNA silencing but contains no HC-Pro. *J. Virol.* **83**, 6934–40.

Mbanzibwa, D.R., Tian, Y.P., Tugume, A.K., et al. (2011) Evolution of cassava brown streak disease-associated viruses. *J. Gen. Virol.* **92**, 974–987.

Michael, W. (2013) African Smallholder Farmers Need to Become Virus Detectors Inter Press Service. *Inter Press Serv.*, 2.

Miras, M., Truniger, V., Querol-Audi, J. and Aranda, M.A. (2017) Analysis of the interacting partners eIF4F and 3′-CITE required for *Melon necrotic spot virus* cap-independent translation. *Mol. Plant Pathol.* **18**, 635–648.

Mohammed, I.U., Abarshi, M.M., Muli, B., Hillocks, R.J. and Maruthi, M.N. (2012) The Symptom and Genetic Diversity of Cassava Brown Streak Viruses Infecting Cassava in East Africa. *Adv. Virol.* **2012**, 1–10.

Moury, B., Charron, C., Janzac, B., Simon, V., Gallois, J.L., Palloix, A. and Caranta, C. (2014) Evolution of plant eukaryotic initiation factor 4E (eIF4E) and potyvirus genome-linked protein (VPg): a game of mirrors impacting resistance spectrum and durability. *Infect. Genet. Evol.* **27**, 472–80.

Mulimbi, W., Phemba, X., Assumani, B., et al. (2012) First report of Ugandan cassava brown streak virus on cassava in Democratic Republic of Congo. *New Dis. Reports* **26**.

Murray, M.G. and Thompson, W.F. (1980) Rapid isolation of high molecular weight plant ONA. *Nucleic Acids Res.*

Odipio, J., Alicai, T., Ingelbrecht, I., Nusinow, D.A., Bart, R.S. and Taylor, N.J. (2017) Efficient CRISPR/Cas9 Genome Editing of Phytoene desaturase in Cassava. *Front. Plant Sci.* **8**.

Ogwok, E., Alicai, T., Rey, M.E.C., Beyene, G. and Taylor, N.J. (2015) Distribution and accumulation of cassava brown streak viruses within infected cassava (Manihot esculenta) plants. *Plant Pathol.* **64**, 1235–1246.

Olspert, A., Chung, B.Y.-W., Atkins, J.F., Carr, J.P. and Firth, A.E. (2015) Transcriptional slippage in the positive-sense RNA virus family Potyviridae. *EMBO Rep.* **16**, 995–1004.

Pan, C., Ye, L., Qin, L., Liu, X., He, Y., Wang, J., Chen, L. and Lu, G. (2016) CRISPR/Cas9-mediated efficient and heritable targeted mutagenesis in tomato plants in the first and later generations. *Sci. Rep.* **6**, 24765.

Patil, B.L., Legg, J.P., Kanju, E. and Fauquet, C.M. (2015) Cassava brown streak disease: a threat to food security in Africa. *J. Gen. Virol.* **96**, 956–968.

Paula De Toledo Thomazella, D., Brail, Q., Dahlbeck, D. and Staskawicz, B. (2016) CRISPR-Cas9 mediated mutagenesis of a DMR6 ortholog in tomato confers broad-spectrum disease resistance. *bioRxiv*.

Peng, R., Lin, G. and Li, J. (2016) Potential pitfalls of CRISPR/Cas9-mediated genome editing.

FEBS J. **283**, 1218–1231.

Piron, F., Nicolaï, M., Minoïa, S., Piednoir, E., Moretti, A., Salgues, A., Zamir, D., Caranta, C. and Bendahmane, A. (2010) An Induced Mutation in Tomato eIF4E Leads to Immunity to Two Potyviruses Nollen, E.A.A., ed. PLoS One 5, e11313.

Pyott, D.E., Sheehan, E. and Molnar, A. (2016) Engineering of CRISPR/Cas9-mediated potyvirus resistance in transgene-free Arabidopsis plants. *Mol. Plant Pathol.* **17**, 1276–1288.

Reddy, A.S.N. (2007) Alternative Splicing of Pre-Messenger RNAs in Plants in the Genomic Era. *Annu. Rev. Plant Biol.* **58**, 267–294.

Revers, F. and García, J.A. (2015) Molecular Biology of Potyviruses. *Adv. Virus Res.* **92**, 101–99.

Revers, F. and Nicaise, V. (2014) Plant Resistance to Infection by Viruses. In eLS., Chichester, UK: John Wiley & Sons, Ltd.

Robaglia, C. and Caranta, C. (2006) Translation initiation factors: a weak link in plant RNA virus infection. *Trends Plant Sci.* **11**, 40–5.

Rodamilans, B., Valli, A., Mingot, A., San León, D., Baulcombe, D., López-Moya, J.J. and García, J.A. (2015) RNA polymerase slippage as a mechanism for the production of frameshift gene products in plant viruses of the potyviridae family. *J. Virol.* **89**, 6965–7.

Ronde, D. de, Butterbach, P. and Kormelink, R. (2014) Dominant resistance against plant viruses. Front. Plant Sci. 5, 307.

Ruffel, S., Gallois, J.-L., Moury, B., Robaglia, C., Palloix, A. and Caranta, C. (2006) Simultaneous mutations in translation initiation factors eIF4E and eIF(iso)4E are required to prevent pepper veinal mottle virus infection of pepper. *J. Gen. Virol.* **87**, 2089–2098.

Ruud, K.A., Kuhlow, C., Goss, D.J. and Browning, K.S. (1998) Identification and characterization of a novel cap-binding protein from Arabidopsis thaliana. *J. Biol. Chem.* **273**, 10325–30.

Schaad, M.C., Anderberg, R.J. and Carrington, J.C. (2000) Strain-Specific Interaction of the Tobacco Etch Virus NIa Protein with the Translation Initiation Factor eIF4E in the Yeast Two-Hybrid System. *Virology* **273**, 300–306.

Schreuder, M.M., Raemakers, C.J.J.M., Jacobsen, E. and Visser, R.G.F. (2001) Efficient production of transgenic plants by Agrobacterium-mediated transformation of cassava (Manihot esculenta Crantz). *Euphytica* **120**, 35–42.

Shi, S., Zhang, X., Mandel, M.A., et al. (2017) Variations of five eIF4E genes across cassava accessions exhibiting tolerant and susceptible responses to cassava brown streak disease Jang, S.K., ed. *PLoS One* **12**, e0181998.

Sievers, F., Wilm, A., Dineen, D., et al. (2014) Fast, scalable generation of high-quality protein multiple sequence alignments using Clustal Omega. *Mol. Syst. Biol.* **7**, 539–539.

Simko, I. and Piepho, H.-P. (2012) The Area Under the Disease Progress Stairs: Calculation, Advantage, and Application. *Phytopathology* **102**, 381–389.

Tamura, K., Stecher, G., Peterson, D., Filipski, A. and Kumar, S. (2013) MEGA6: Molecular Evolutionary Genetics Analysis version 6.0. *Mol. Biol. Evol.* **30**, 2725–9.

Taylor, N., Gaitán-Solís, E., Moll, T., et al. (2012) A High-throughput Platform for the Production and Analysis of Transgenic Cassava (Manihot esculenta) Plants. *Trop. Plant Biol.* **5**, 127–139.

Taylor, N.J., Edwards, M., Kiernan, R.J., Davey, C.D., Blakesley, D. and Henshaw, G.G. (1996) Development of friable embryogenic callus and embryogenic suspension culture systems in cassava (Manihot esculenta Crantz). *Nat. Biotechnol.* **14**, 726–30.

Voytas, D.F. (2013) Plant Genome Engineering with Sequence-Specific Nucleases. *Annu. Rev. Plant Biol.* **64**, 327–350.

Wagaba, H., Beyene, G., Trembley, C., Alicai, T., Fauquet, C.M. and Taylor, N.J. (2013) Efficient transmission of cassava brown streak disease viral pathogens by chip bud grafting. *BMC Res. Notes* **6**, 516.

Wang, A. (2015) Dissecting the Molecular Network of Virus-Plant Interactions: The Complex Roles of Host Factors. *Annu. Rev. Phytopathol.* 53, 45–66.

Wang, A. and Krishnaswamy, S. (2012) Eukaryotic translation initiation factor 4E-mediated recessive resistance to plant viruses and its utility in crop improvement. *Mol. Plant Pathol.* **13**, 795–803.

Wang, Y., Cheng, X., Shan, Q., Zhang, Y., Liu, J., Gao, C. and Qiu, J.-L. (2014) Simultaneous editing of three homoeoalleles in hexaploid bread wheat confers heritable resistance to powdery mildew. *Nat. Biotechnol.* **32**, 947–951.

Wilson, M.C., Mutka, A.M., Hummel, A.W., et al. (2017) Gene expression atlas for the food security crop cassava. *New Phytol.* **213**, 1632–1641.

Wittmann, S., Chatel, H., Fortin, M.G. and Laliberté, J.-F.F. (1997) Interaction of the viral protein genome linked of turnip mosaic potyvirus with the translational eukaryotic initiation factor (iso) 4E of Arabidopsis thaliana using the yeast two-hybrid system. *Virology* **234**, 84–92.

Yeam, I., Cavatorta, J.R., Ripoll, D.R., Kang, B.-C. and Jahn, M.M. (2007) Functional Dissection of Naturally Occurring Amino Acid Substitutions in eIF4E That Confers Recessive Potyvirus Resistance in Plants. *PLANT CELL ONLINE* **19**, 2913–2928.

Zhang, H., Zhang, J., Wei, P., et al. (2014) The CRISPR/Cas9 system produces specific and homozygous targeted gene editing in rice in one generation. Plant Biotechnol. J. 12, 797–807.

Zhang, Y.-Y., Li, H.-X., Ouyang, B. and Ye, Z.-B. (2006) Regulation of Eukaryotic Initiation Factor 4E and Its Isoform: Implications for Antiviral Strategy in Plants. *J. Integr. Plant Biol.* **48**, 1129–1139.

Supporting Information legends

Figure S1. Roles of host eIF4E-potyvirus VPg interaction and sources of recessive resistance. (a) Linkage of potyvirus VPg to its binding site on eIF4E can provide translation initiation via recruitment of necessary factors and ribosomal subunits, genomic stability via protection from host-encoded exonucleases, and intracellular trafficking via eIF4G microtubule binding activity. (b) Non-conservative amino acid changes and gene deletions that abolish VPg-eIF4E binding removes above described roles, therefore conferring recessive resistance

Figure S2. CRISPR/Cas9-induced mutagenesis evident in *nCBP-1* (a) and *nCBP-2* (b) via restriction enzyme site loss (RESL). PCR amplicons of targeted regions were digested with SmlI. Map of amplicons with nCBP exon (purple), protospacer adjacent motif (red), gRNA spacer (green), predicted Cas9 cut site (black arrow), and overlapping SmlI restriction enzyme recognition site (bold, red). Bands are measured relative to O'Gene Ruler 1 kb Plus Ladder. Experimental banding pattern is consistent with predicted RESL.

Figure S3. CRISPR/Cas9 –induced mutagenesis creates out of frame alternate splice variants. Exon 1 and exon 2 splice junction of nCBP-1 (a) and nCBP-2 (b) were examined via sequence analysis of cDNA. Predicted Cas9 cut site is shown as a black arrow. STOP codon is shown as starred, red box.

Figure S4. *ncbp-1/ncbp-2* double mutants exhibit reduced UCBSV symptom incidence and delayed CBSV symptom onset
(a), (b), aerial symptom incidence reported as percent of wild type, *ncbp-1*, *ncbp-2*, or *ncbp-1/ncbp-2* plants bud-graft inoculated with UCBSV T04 ($n \geq 10$). (c), (d), aerial symptom incidence as previously described in plants inoculated with CBSV Naliendele ($n \geq 7$).

Figure S5. *ncbp-1/ncbp-2* double mutants exhibit reduced aerial CBSV symptom severity
(a), (b), disease progression curves of wild type, *ncbp-1*, *ncbp-2*, or *ncbp-1/ncbp-2* plants bud-graft inoculated with CBSV Naliendele ($n \geq 7$). Leaf and stem symptoms were each scored on a 0-4 scale and summed to obtain an aggregate aerial score. (c), (d), average <u>a</u>rea <u>u</u>nder the <u>d</u>isease <u>p</u>rogression <u>c</u>urve (AUDPC) derived from data plotted in A and B. Error bars indicate standard error of the mean. Statistical differences were detected by Welch's t-test, $\alpha=0.05$, *≤0.05, **≤0.01, ****≤0.0001.

Figure S6. *ncbp-1/ncbp-2* double mutant stem symptom severity is consistently reduced across all experiments
Separate leaf and stem disease progression curves for wild type, *ncbp-1*, *ncbp-2*, or *ncbp-1/ncbp-2* plants bud-graft inoculated with CBSV Naliendele ($n \geq 7$). Leaf and stem symptoms were each scored on a 0-4 scale. (a), (c), and (e) represent leaf disease progression curves from three different experiments while (b), (d), and (f) represent corresponding stem disease progression curves. Error bars represent standard error of the mean.

Figure S7. 12-2016 CBSV challenge leaf symptom severity is similar across all genotypes
Wild type, *ncbp-1*, *ncbp-2*, or *ncbp-1/2* plants bud-graft inoculated with CBSV Naliendele isolate all develop widespread chlorotic leaf symptoms. Leaf images were taken near 12-2016 challenge endpoint. Scale bar denotes 1 cm.

Figure S8. *nCBP-2* is highly expressed in storage roots
Heat map describing tissue specific expression of cassava *eIF4E* isoforms. Data was extracted from the Bart Lab Cassava Atlas (http://shiny.danforthcenter.org/cassava_atlas/). Expression values are defined as fragments per kilobase of transcript per million mapped reads (FPKM).

Fig S9. 6-2016 UCBSV challenge virus titer analysis
Quantitative real time PCR analysis of UCBSV T04 titer in wild type, *ncbp-1/2* #2, and *ncbp-1/2* #8 leaf tissue. Leaf samples were collected from the first fully expanded leaf at each time-point. n≥6 per genotype. Whiskers span the interquartile range, solid bars indicate the median of scores.

Figure legends

Figure 1. Identification of cassava eIF4E family homologs.
(a) Phylogenetic relationships of cassava eIF4E family with *A. thaliana*, At, eIF4E family inferred by the Maximum Likelihood method based on the Le_Gascuel_2008 model (Le and Gascuel, 1993). The percentage of trees in which the associated taxa clustered together is shown next to the branches. The tree is drawn to scale, with branch lengths measured in the number of substitutions per site. Tree rooted to *Homo sapiens*, Hs, eIF4E-3. (b) Percent identity matrix of cassava eIF4E family with At eIF4E family using amino acid sequences. (c) Descriptions of cassava eIF4E family based upon phylogenetic relationships and percent identity matrix.

Figure 2. CBSV and UCBSV VPgs interact with cassava nCBP-1 and nCBP-2.
Yeast two-hybrid constructs consist of B42 activation domain (AD) fused to the CBSV Naliendele VPg and UCBSV T04 VPg, and LexA DNA binding domain (BD) bound to cassava eIF4E family members. Blue coloration represents β-galactosidase activity from activation of lacZ reporter gene by protein-protein interaction. Five yeast transformants are displayed on the dropout medium SD Gal/Raf SD-UTH. Positive control is shown in the dashed red box (TuMV VPg-AD and *A. thaliana* eIF(iso)4E-BD).

Figure 3. Method for generating CRISPR/Cas9 mediated gene edited cassava plants.
(a) Transgenic cassava are produced via *Agrobacterium*-mediated transformation of friable embryogenic callus (FECs). 1) FECs are induced from somatic tissues by placing the latter on growth media supplemented with picloram. FECs are comprised of aggregated spheroid embryogenic units. Individual units (boxed in panel 1 and enlarged in panel 2) range from a few cells to approximately 1 mm in diameter. 2) FECs are transformed with CRISPR/Cas9 constructs through co-culture with *Agrobacterium tumefaciens.* Red semi-circles denote T-DNA fragments and red spheres denote transformed cells. 3) Cells on the surface of embryogenic units, transformed or untransformed, divide to produce new embryogenic units. CRISPR/Cas9

editing can occur prior to or after division. Edited cells are colored purple. 4) Antibiotic selection kills untransformed daughter embryoids. Dead cells marked with "X". Transformed embryogenic units are spread over selective media and form colonies. One mature embryo per colony is recovered (5), and develops into a plantlet (6). Each regenerated plant is clonally propagated and referred to as a mutant line. (b) Workflow for mutant genotype characterization and line selection.

Figure 4. Cas9 induces INDELs at *nCBP-1* and *nCBP-2* gRNA target sites in *nCBP-1/2* transgenic lines.
(a) Sequences at the junction of the first exon-intron boundary were selected for targeting of the Cas9 nuclease. Lengths of *nCBP-1* and *nCBP-2* genes are to nucleotide scale (top bar). Exons are denoted by solid blocks and introns are represented as dashed lines. Arrowheads indicate the 3' terminus. (b) Diagram of the protospacer adjacent motif (PAM) and guide RNA (gRNA) targeting *nCBP-1*. (c) Diagram of the PAM and gRNA targeting *nCBP-2*. (d) INDELs of *nCBP-1* and *nCBP-2* in mutant lines *nCBP-1* #-1, *nCBP-2* #6, *nCBP-1/2* #2, and *nCBP-1/2* #8. Upper and lower cases denote exonic and intronic sequence, respectively. Red boxes indicate INDELs.

Figure 5. Alternative splicing of *nCBP-1* generates variants that maintain the downstream reading frame.
(a) Schematic of canonical and alternative nCBP-1 splice sites. Boxed region of the nCBP-1 gene model is enlarged below. Exon and intron sequences are given in capital and small letters, respectively. Green and red boxes highlight splice motifs at the 5' and 3' end of introns, respectively. Type 1 splicing produces the predicted wild type nCBP-1 cDNA sequence. Type 2 and 3 splicing are observed in ncbp-1/2 lines #2 & #8, respectively. (b) cDNA sequences detected in clone-seq experiments. Red boxes denote INDELs resulting from both CRISPR/Cas9-mediated edits and alternative splicing. In ncbp-1/2 #2, type 2 splicing results in retention of 3' sequence from intron 1 of one ncbp-1 allele (1 of 9 clones sequenced). In ncbp-1/2 #8, an INDEL disrupting the canonical splice motif between exon 1 and intron 1 of ncbp-1 results in a type 3 splice variant (4 of 6 clones sequenced).

Figure 6. *ncbp-1/ncbp-2* double mutants exhibit delayed CBSV symptom onset and reduced symptom severity
(a), (b) Aerial symptom incidence reported as percent of wild type, *ncbp-1*, *ncbp-2*, or *ncbp-1/ncbp-2* plants (n≥5) bud-graft inoculated with either CBSV Naliendele or UCBSV T04 isolates, respectively. *ncbp-1/ncbp-2* double mutant lines #2 and #8 are the product of independent transgenic events. (c) Disease progression curves for previously described CBSV inoculated plants. Leaf and stem symptoms were each scored on a 0-4 scale and summed to obtain an aggregate aerial score. (d) Average area under the disease progression curve (AUDPC) derived from data plotted in (c). Error bars in (c) and (d) indicate standard error of the mean. Statistical differences were detected by Welch's t-test, $\alpha=0.05$, *≤0.05, **≤0.01, ****≤0.0001.

Figure 7. CBSD stem symptom attenuation on *ncbp-1/ncbp-2* double mutants.
(a) Representative wild type, *ncbp-1*, *ncbp-2*, or *ncbp-1/ncbp-2* stems displaying varying degrees of brown streak symptoms 14 weeks post graft inoculation with CBSV Naliendele. *ncbp-1/ncbp-2* double mutants present reduced brown streaking and associated dark pigmentation along the length their stems. Portions of stems boxed in red are enlarged in (b). Imaged portions of stems are all approximately the same distance above the graft site.

Figure 8. *ncbp-1/ncbp-2* double mutant storage roots are less symptomatic and accumulate less virus.
(a) Storage root sections were assessed on a 1-5 scale, where 1 corresponds with no symptoms and 5 with extensive necrosis present throughout the diameter of root. (b) *ncbp-1/2* storage roots are significantly less symptomatic than wild type at 12 to 14 weeks post bud-graft inoculation with CBSV Naliendele isolate. Points represent average scores of all storage root sections from a single plant. Data from three experimental replicates were pooled. Whiskers span the interquartile range, solid bars indicate the median of scores, + indicates the mean of scores. Statistical significance was detected by Welch's t-test, $n \geq 19$, $\alpha = 0.05$. (c) Quantitative real time PCR analysis reveals that *ncbp-1/2* storage roots accumulate less virus than wild type. CBSV *HAM1-LIKE* was normalized to *PP2A4*. Data from three experimental replicates were pooled. Significant differences were detected with a Mann-Whitney U-test, $n \geq 19$, $\alpha = 0.05$, *≤0.05, **≤0.01, ****≤0.0001.

a.

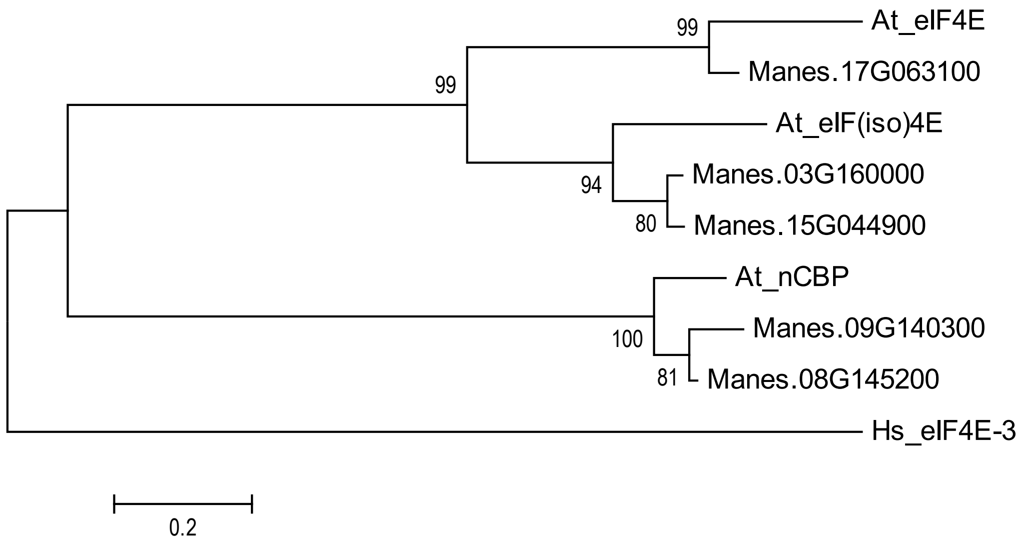

b.

	Hs_eIF4E-3	At_nCBP	Manes.08G145200	Manes.09G140300	At_eIF4E	Manes.17G063100	At_eIF(iso)4E	Manes.03G160000	Manes.15G044900
Hs_eIF4E-3	100.00								
At_nCBP	30.46	100.00							
Manes.08G145200	30.29	77.38	100.00						
Manes.09G140300	30.86	74.09	88.34	100.00					
At_eIF4E	29.48	29.49	30.80	28.77	100.00				
Manes.17G063100	31.21	28.37	29.73	28.11	68.24	100.00			
At_eIF(iso)4E	29.17	31.55	31.05	29.95	47.67	50.26	100.00		
Manes.03G160000	33.53	30.89	30.93	30.89	50.25	53.33	69.43	100.00	
Manes.15G044900	33.53	31.41	30.41	30.89	49.75	55.38	69.43	92.50	100.00

c.

Locus Name	Description
Manes.17G063100	eIF4E
Manes.03G160000	eIF(iso)4E-1
Manes.15G044900	eIF(iso)4E-2
Manes.09G140300	nCBP-1
Manes.08G145200	nCBP-2

Figure 1. Identification of cassava eIF4E family homologs. (A) Phylogenetic relationships of cassava eIF4E family with *Arabidopsis thaliana*, At, eIF4E family inferred by the Maximum Likelihood method based on the Le_Gascuel_2008 model (Le and Gascuel, 1993). The percentage of trees in which the associated taxa clustered together is shown next to the branches. The tree is drawn to scale, with branch lengths measured in the number of substitutions per site. Tree is rooted to *Homo sapiens*, Hs, eIF4E-3. (B) Percent identity matrix of cassava eIF4E family with At eIF4E family using amino acid sequences. (C) Descriptions of cassava eIF4E family based upon phylogenetic relationships and percent identity matrix.

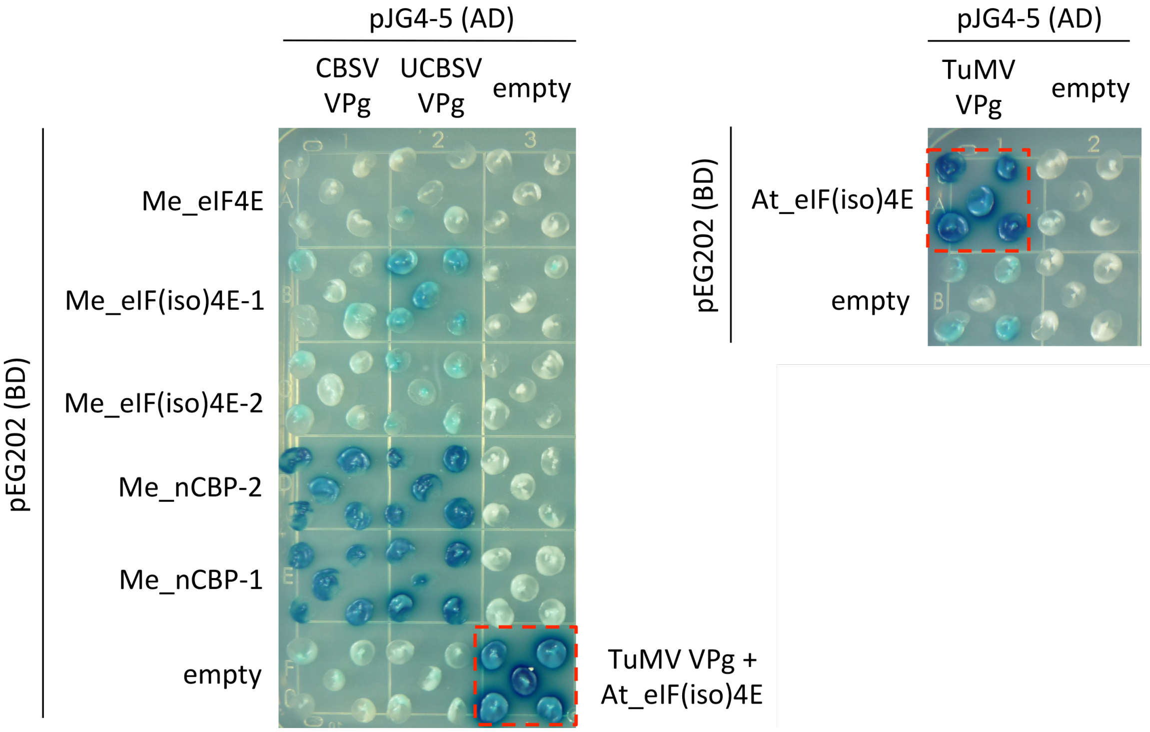

Figure 2. CBSV and UCBSV VPg's interact with cassava nCBP-1 and nCBP-2. Yeast two-hybrid constructs consist of B42 activation domain (AD) is fused to the CBSV Naliendele VPg and UCBSV T04 VPg, and LexA DNA binding domain (BD) bound to cassava eIF4E family members. Blue coloration represents β-galactosidase activity from activation of lacZ reporter gene by protein-protein interaction. Five yeast transformants are displayed on the dropout medium SD Gal/Raf SD-UTH. Positive control is shown in the dashed red box (TuMV VPg-AD and *Arabidopsis thaliana* eIF(iso)4E-BD).

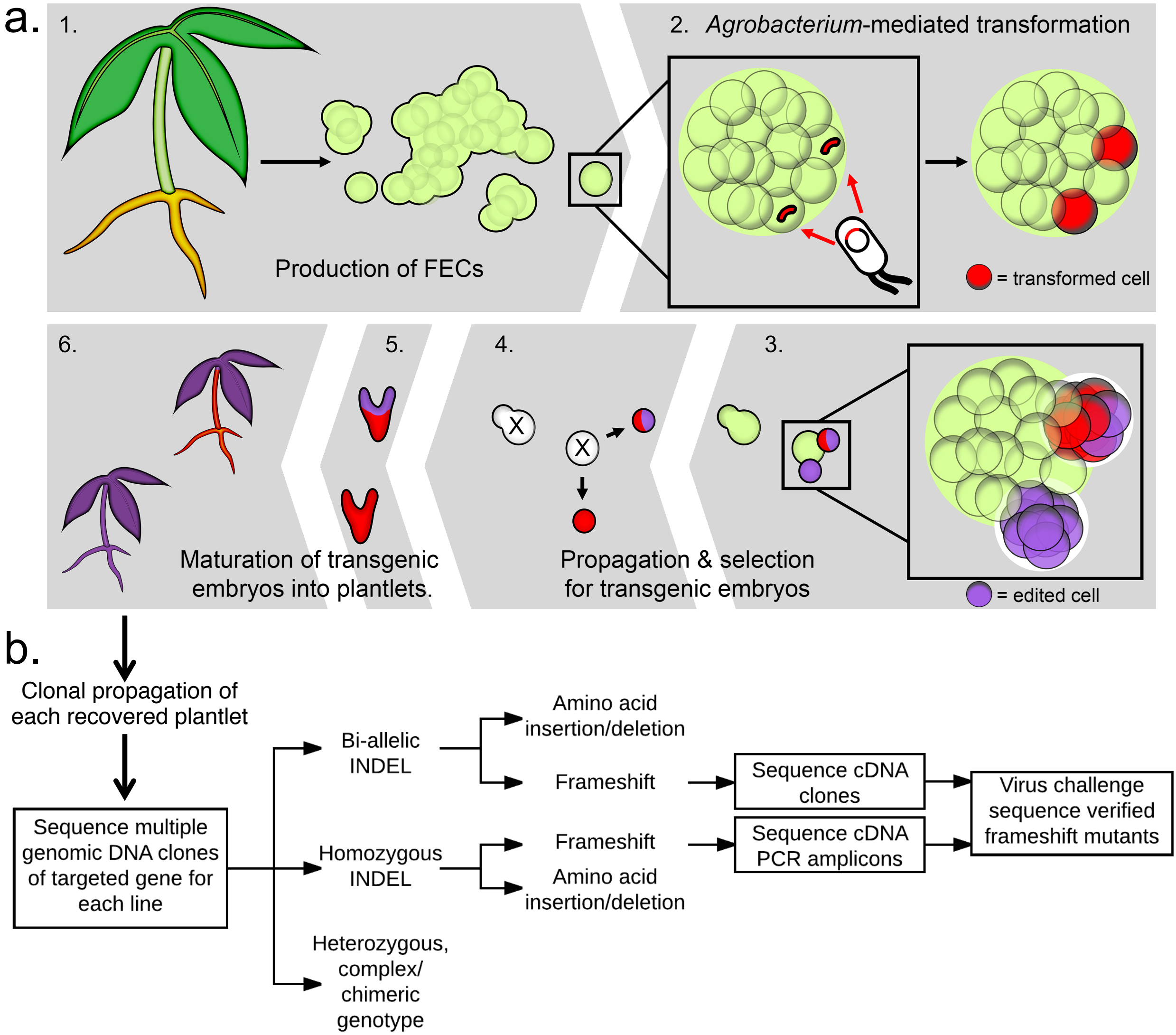

Figure 3. Method for generating CRISPR/Cas9 mediated gene edited cassava
(a) Transgenic cassava are produced via *Agrobacterium*-mediated transformation of friable embryogenic calli (FEC). 1) FEC are induced from somatic tissues by placing the latter on growth media supplemented with picloram. FEC are comprised of aggregated spheroid embryogenic units. Individual units (boxed in panel 1 and enlarged in panel 2) range from a few cells to 1 mm in diameter. 2) FEC are transformed with CRISPR/Cas9 constructs through co-culture with *Agrobacterium tumefaciens.* Red semi-circles denote TDNA fragments and red spheres denote transformed cells. 3) Cells on the surface of embryogenic units, transformed or untransformed, divide to produce new embryogenic units. CRISPR/Cas9 editing can occur prior to or after division. Edited cells are colored purple. 4) Antibiotic selection kills mother and untransformed daughter embryoids. Dead cells marked with "X". Transformed embryogenic units are spread over selective media and form colonies. One mature embryo per colony is recovered (5), and develops into a plantlet (6). Each regenerated plant is clonally propagated and referred to as a mutant line. (b) Workflow for mutant genotype characterization and line selection.

Figure 4. Cas9 induces INDELs at *nCBP-1* and *nCBP-2* gRNA target sites in BS05 transgenic line. (a) Sequences at the junction of the first exon-intron boundary were selected for targeting of the Cas9 nuclease. Lengths of nCBP-1 and nCBP-2 genes are to nucleotide scale (top bar). Exons are denoted by solid blocks and introns are represented as dashed lines. Arrowheads indicate the 3' terminus. (b) Diagram of the protospacer adjacent motif (PAM) and guide RNA (gRNA) targeting *nCBP-1*. (c) Diagram of the PAM and gRNA targeting *nCBP-2*. (d) INDELs of *nCBP-1* and *nCBP-2* in mutant lines BS01 #1, BS02 #6, BS05 #2, and BS05 #8. Upper and lower cases denote exonic and intronic sequence, respectively. Red boxes indicate INDELs.

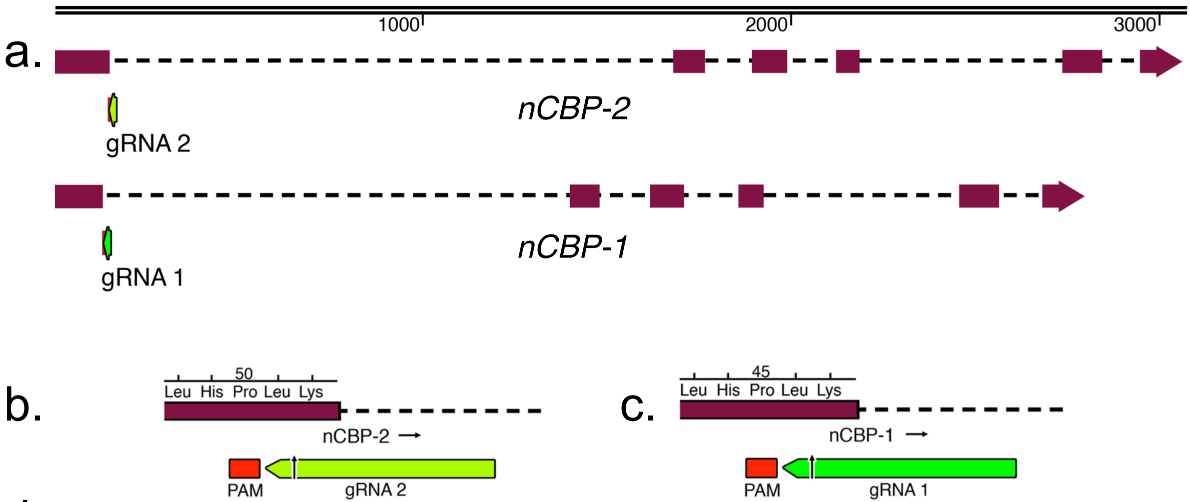

d.

Line:		*nCBP-2* sequence		In frame? :		*nCBP-1* sequence		In frame?
WT	141	TTGCATCCTCTCAAGgttctctctttcgc	170	Y	126	TTGCATCCTCTCA AGgttctcgcttcctc	155	Y
ncbp-1 #1		TTGCATCCTCTCAAGgttctctctttcgc		Y		TTGCATCCTCTCA ---ttctcgcttcctc		N
ncbp-2 #6		TTGCATCCTCTCA-Ggttctctctttcgc		N		TTGCATCCTCTCA AGgttctcgcttcctc		Y
ncbp-1/2 #2		TTGCATCCTCTC-----------tttcgc		N		TTGCATCCTCTCAAAGgttctcgcttcctc		N
ncbp-1/2 #8		TTGCATCCTCTCA-Ggttctctctttcgc		N		TTGCATCCTCTCA ---ttctcgcttcctc		N
						TTGCATCCTCTCA -Ggttctcgcttcctc		N

Table 1. Genotype counts of transgenic T_0 cassava lines.

Construct	**Gene Target**	**Total # of lines**	**Homozygous**	**Bi-allelic**	**Heterozygous**	**Complex/ Chimeric**	**WT**
BS01	*nCBP-1*	6	2	1	0	2	1
BS02	*nCBP-2*	6	1	3	0	2	0
BS03	*nCBP-1*	10	4	5	0	0	1
BS04	*nCBP-2*	15	2	10	1	1	1
BS05	*nCBP-1/2*	8	1	6	0	0	1
BS06	*eIF4E*	7	3	4	0	0	0
BS07	*eIF4E*	3	0	2	0	0	1
	Total	*55*	*13*	*31*	*1*	*5*	*5*
	Percent	*100%*	*24%*	*56%*	*2%*	*9%*	*9%*
	Combined Percentages		*91%*				
			80%				

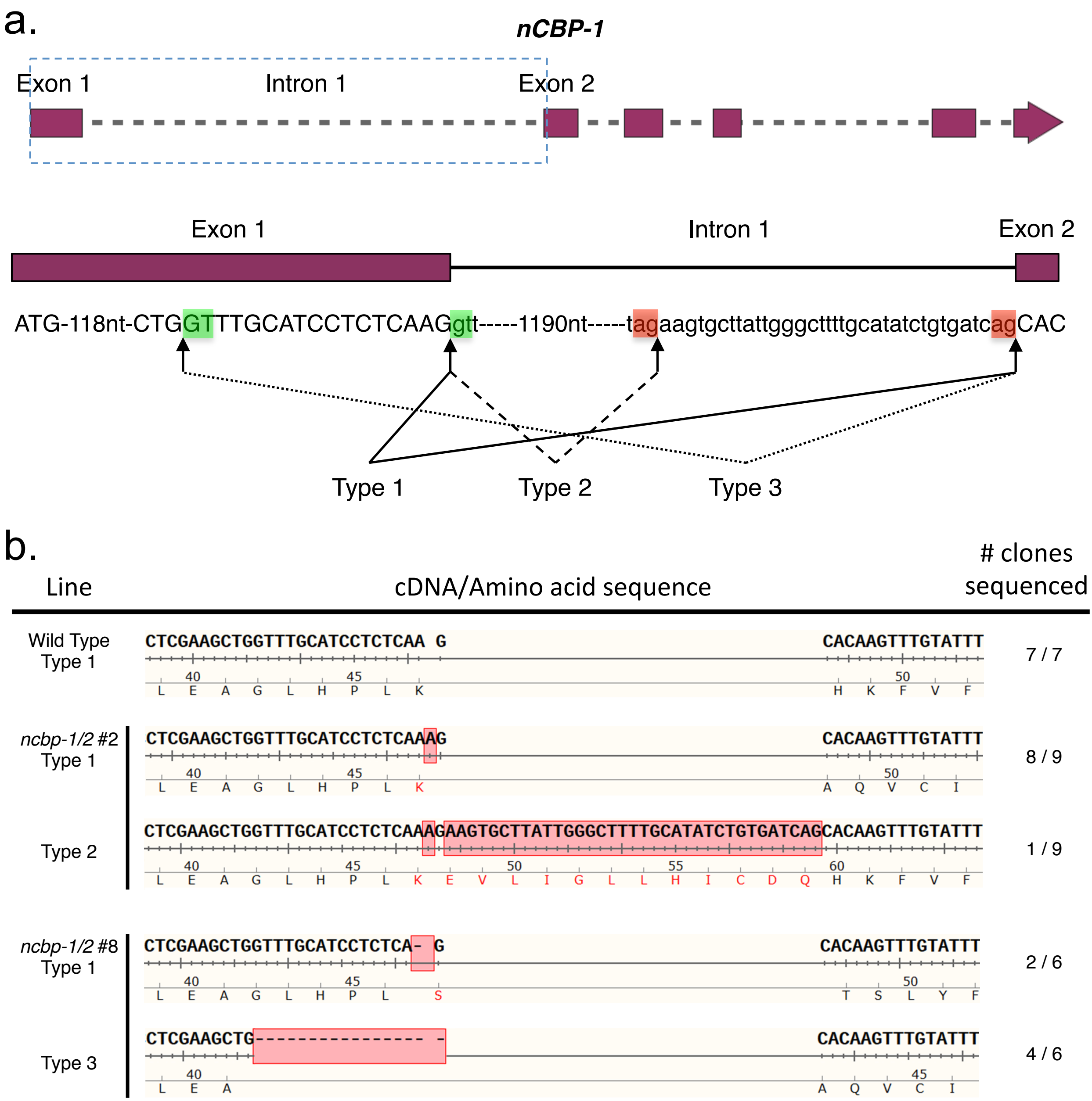

Figure 5. Alternative splicing of *ncbp-1* alleles is detected in *ncbp-1/2* double mutants
(a) Schematic of canonical and alternative *nCBP-1* splice sites. Boxed region of the *nCBP-1* gene model is enlarged below. Exon and intron sequences are given in capital and small letters, respectively. Green and red boxes highlight splice motifs at the 5' and 3' end of introns, respectively. Type 1 splicing produces the predicted wild type *nCBP-1* cDNA sequence. Type 2 and 3 splicing are observed in *ncbp-1/2* lines #2 & #8, respectively. (b) cDNA sequences detected in clone-seq experiments. Red boxes denote INDELs resulting from both CRISPR/Cas9-mediated edits and alternative splicing. In *ncbp-1/2* #2, type 2 splicing results in retention of 3' sequence from intron 1 of one *ncbp-1* allele (1 of 9 clones sequenced). In *ncbp-1/2* #8, an INDEL disrupting the canonical splice motif between exon 1 and intron 1 of *ncbp-1* results in a type 3 splice variant (4 of 6 clones sequenced).

Table 2. Aerial symptom scoring scale

Leaf symptoms	Score	Shoot symptoms
Asymptomatic	**0**	Asymptomatic
Specks of chlorosis localized to a small section of leaf	**1**	Punctate brown streaks localized to small length of stem
Widespread chlorosis throughout leaves	**2**	Spreading brown streaks along less than 10% of the stem
Widespread chlorosis accompanied by slight die-back of terminal branches	**3**	Brown streaking along 10-60% of stem
Widespread chlorosis and plant die-back	**4**	Continuous brown streaking along the entire stem length

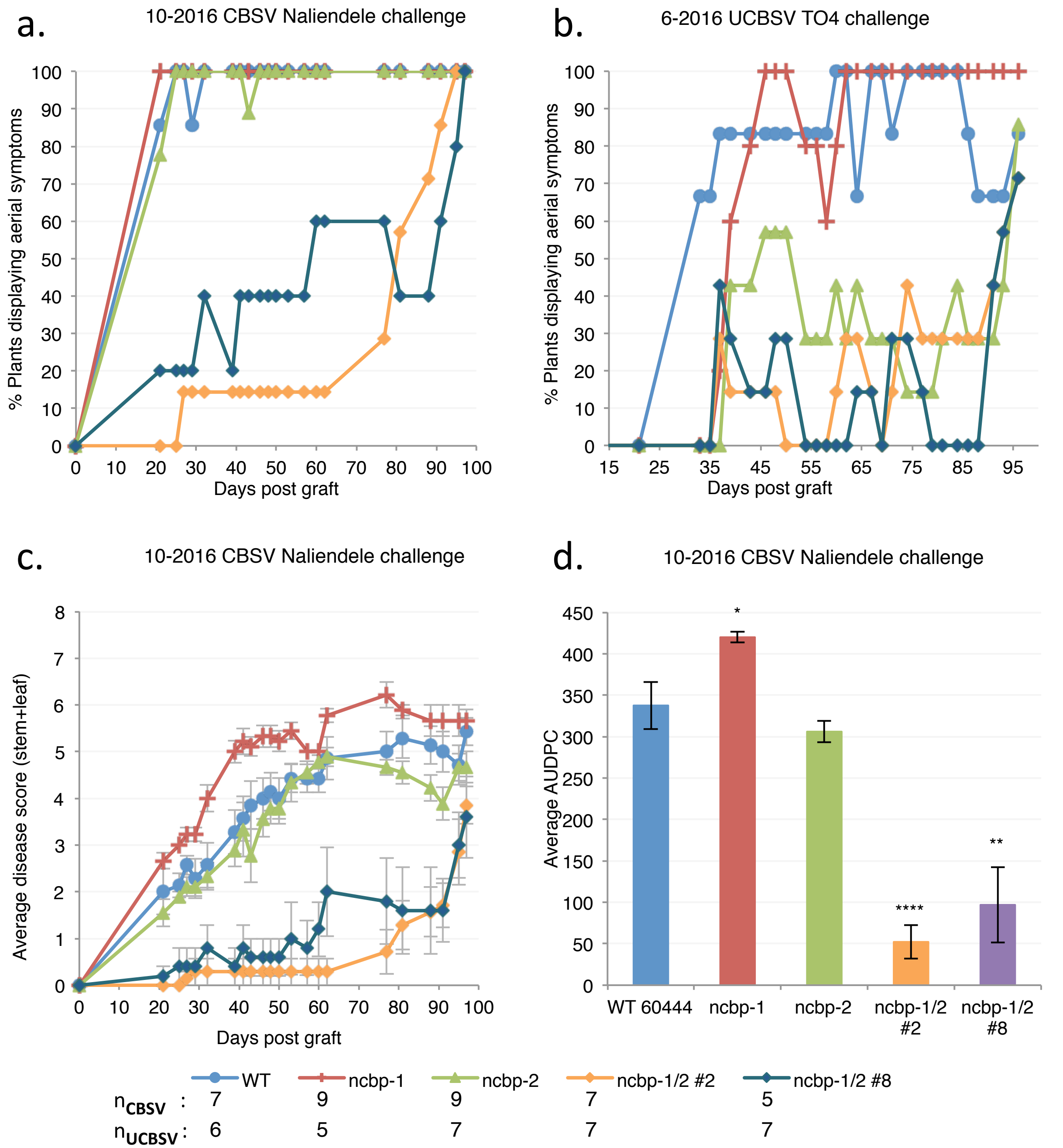

Figure 6. *ncbp-1 ncbp-2* double mutants exhibit delayed CBSV symptom onset and reduced symptom severity (a), (b), aerial symptom incidence reported as percent of wild type, *ncbp-1*, *ncbp-2*, or *ncbp-1 ncbp-2* plants bud-graft inoculated with either CBSV Naliendele or UCBSV T04 (n≥5) isolates, respectively. *ncbp-1 ncbp-2* double mutant lines #2 and #8 are the product of independent transgenic events. (c), disease progression curves for previously described CBSV inoculated plants. Leaf and stem symptoms were each scored on a 0-4 scale and summed to obtain an aggregate aerial score. (d), average area under the disease progression curve (AUDPC) derived from data plotted in C. Error bars in C and D indicate standard error of the mean. Statistical differences were detected by Welch's t-test, α=0.05, *≤0.05, **≤0.01, ****≤0.0001.

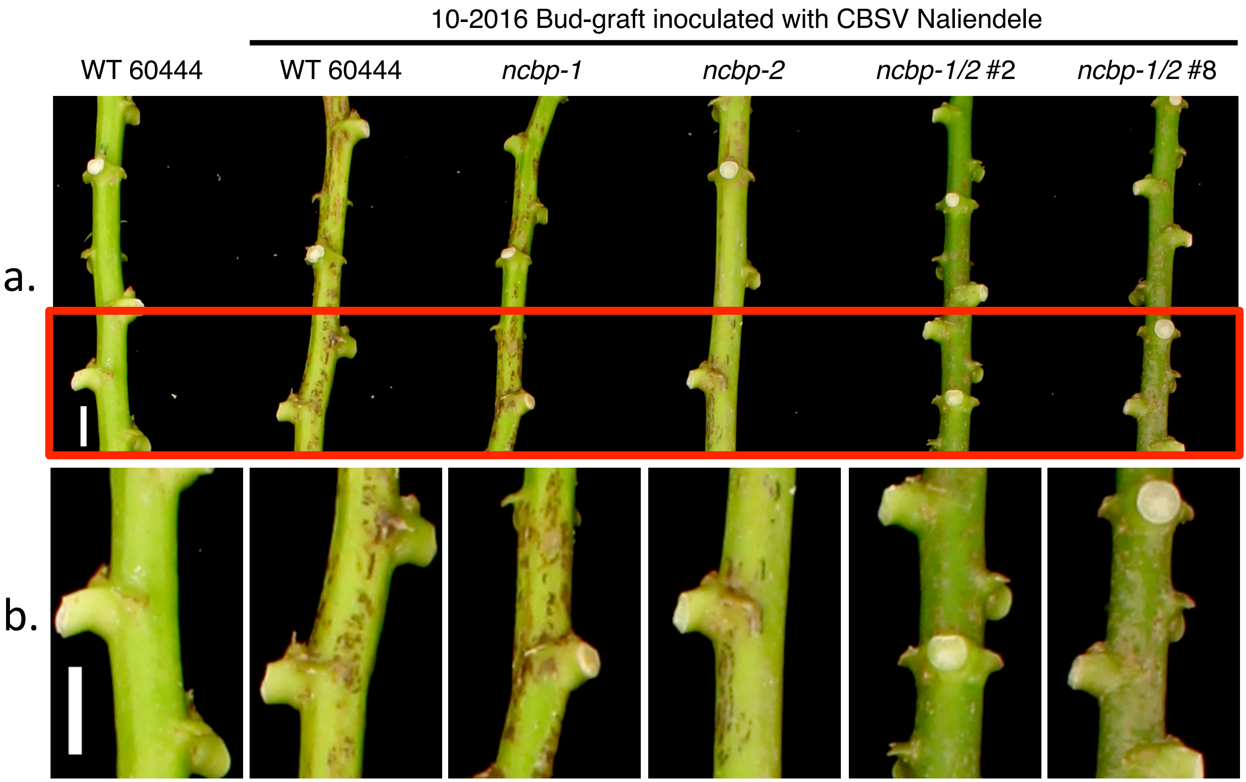

Figure 7. CBSD stem symptom attenuation on *ncbp-1 ncbp-2* double mutants
(a), representative wild type, *ncbp-1*, *ncbp-2*, or *ncbp-1 ncbp-2* stems displaying varying degrees of brown streak 14 weeks post graft inoculation with CBSV Naliendele. *ncbp-1 ncbp-2* double mutants present reduced brown streaking and associated dark pigmentation along the length their stems. Portions of stems boxed in red are enlarged in (b). Imaged portions of stems are all approximately the same distance from the graft site.

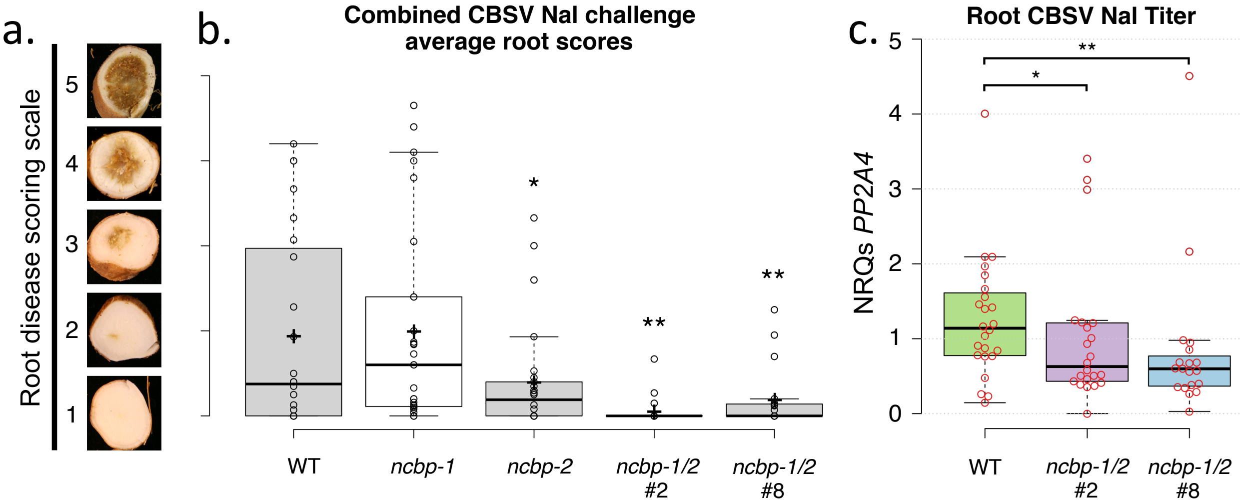

Figure 8. *ncbp-1 ncbp-2* double mutant storage roots are less symptomatic and accumulate less virus (a), storage root sections were assessed on a 1-5 scale, 1 corresponding with asymptomatic and 5 corresponding with extensive necrosis present throughout the diameter of root. (b), *ncbp-1 ncbp-2* storage roots are significantly less symptomatic than wild type at 12 to 14 weeks post bud-graft inoculation with CBSV Naliendele isolate. Points represent average scores of all storage root sections from a single plant. Data from three experimental replicates were pooled. Whiskers span the interquartile range, solid bars indicate the median of scores, + indicates the mean of scores. Statistical significance was detected by Welch's t-test, n≥19, α=0.05, *≤0.05, **≤0.01, ****≤0.0001. (c), quantitative real time PCR analysis reveals that *ncbp-1/2* storage roots accumulate less virus than wild type. CBSV *HAM1-LIKE* was normalized to *PP2A4*. Data from three experimental replicates were pooled. Significant differences were detected with a Mann-Whitney U-test, n≥19, α=0.05.

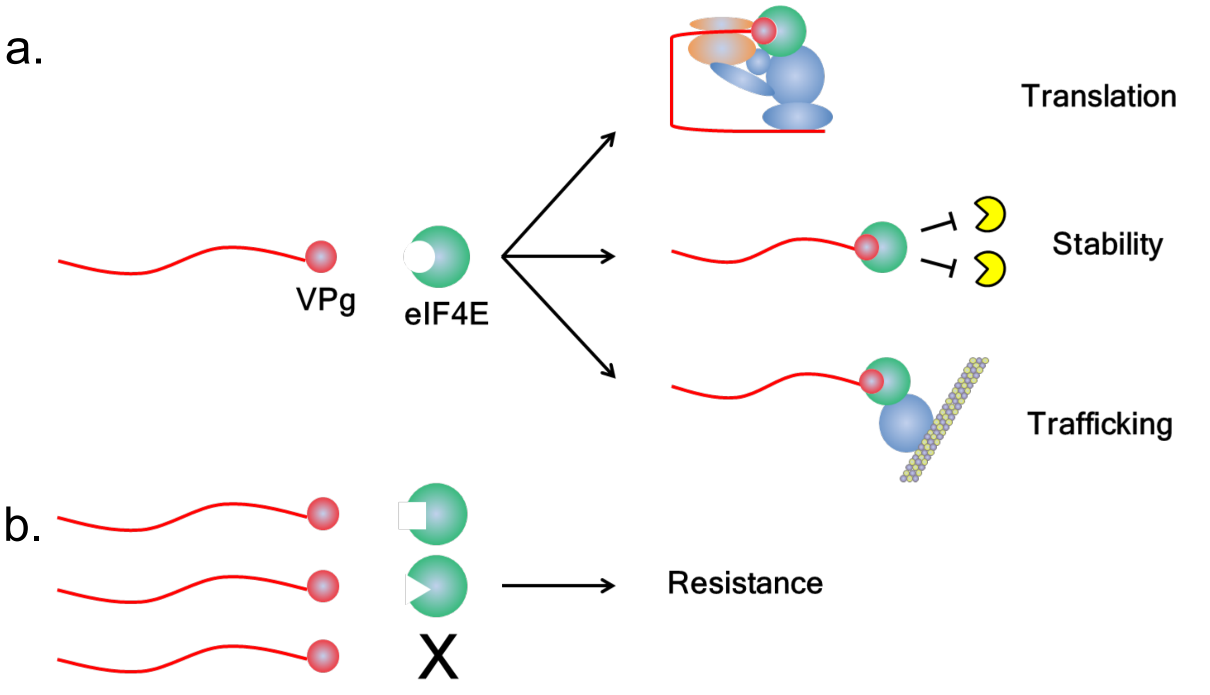

Figure S1. Roles of host eIF4E-potyvirus VPg interaction and sources of recessive resistance. (a) Linkage of potyvirus VPg to its binding site on eIF4E can provide translation initiation via recruitment of necessary factors and ribosomal subunits, genomic stability via protection from host-encoded exonucleases, and intracellular trafficking via eIF4G microtubule binding activity. (b) Non-conservative amino acid changes and gene deletions that abolish VPg-eIF4E binding removes above described roles, therefore conferring recessive resistance.

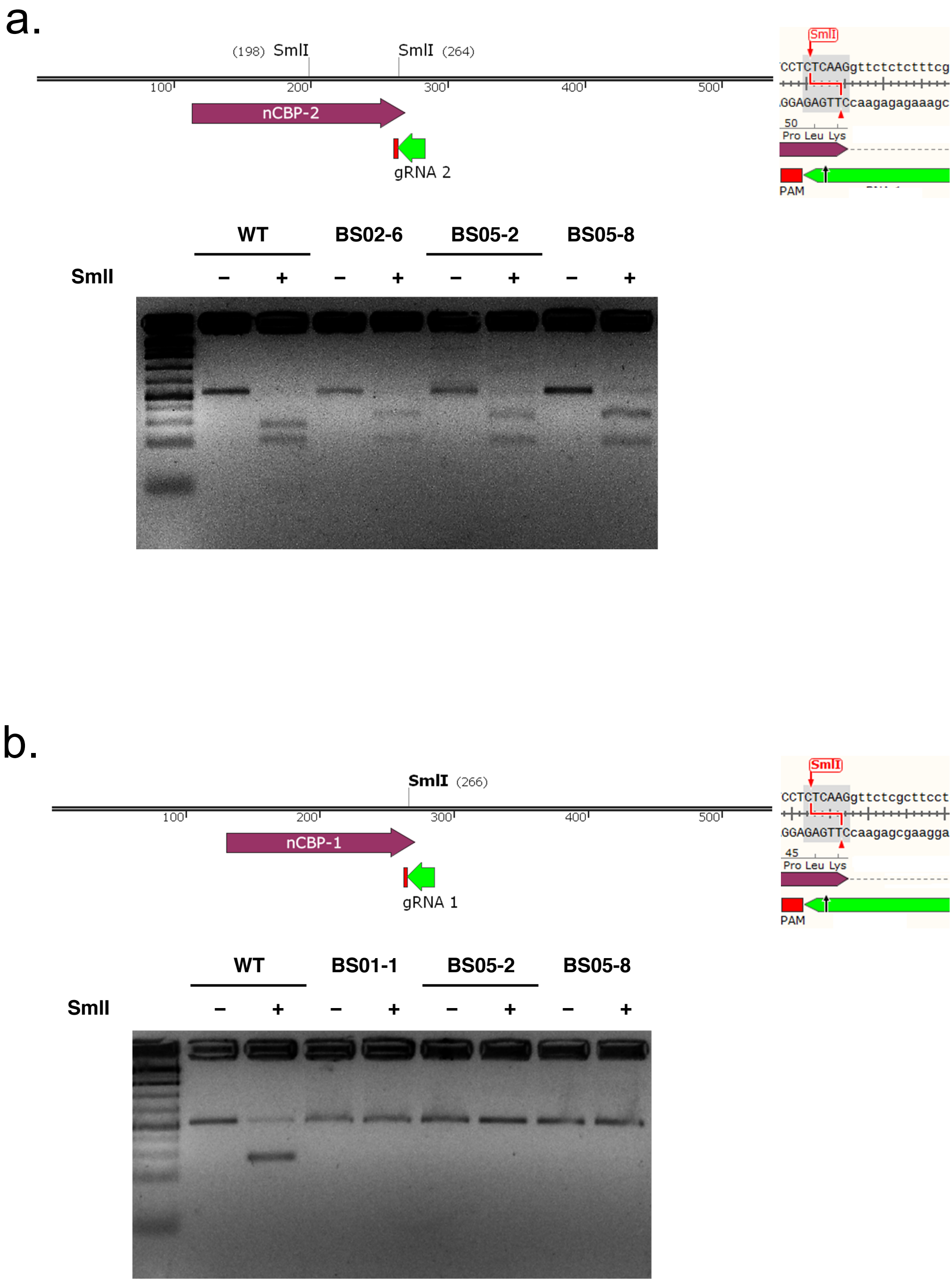

Figure S2. CRISPR-induced mutagenesis evident in nCBP-1 (a) and nCBP-2 (b) via restriction enzyme site loss (RESL). PCR amplicons of targeted regions were digested with SmlI. Map of amplicons with nCBP exon (purple), protospacer adjacent motif (red), gRNA spacer (green), predicted Cas9 cut site (black arrow), and overlapping SmlI restriction enzyme recognition site (bold, red). Bands are measured relative to O'Gene Ruler 1 kb Plus Ladder. Experimental banding pattern is consistent with predicted RESL.

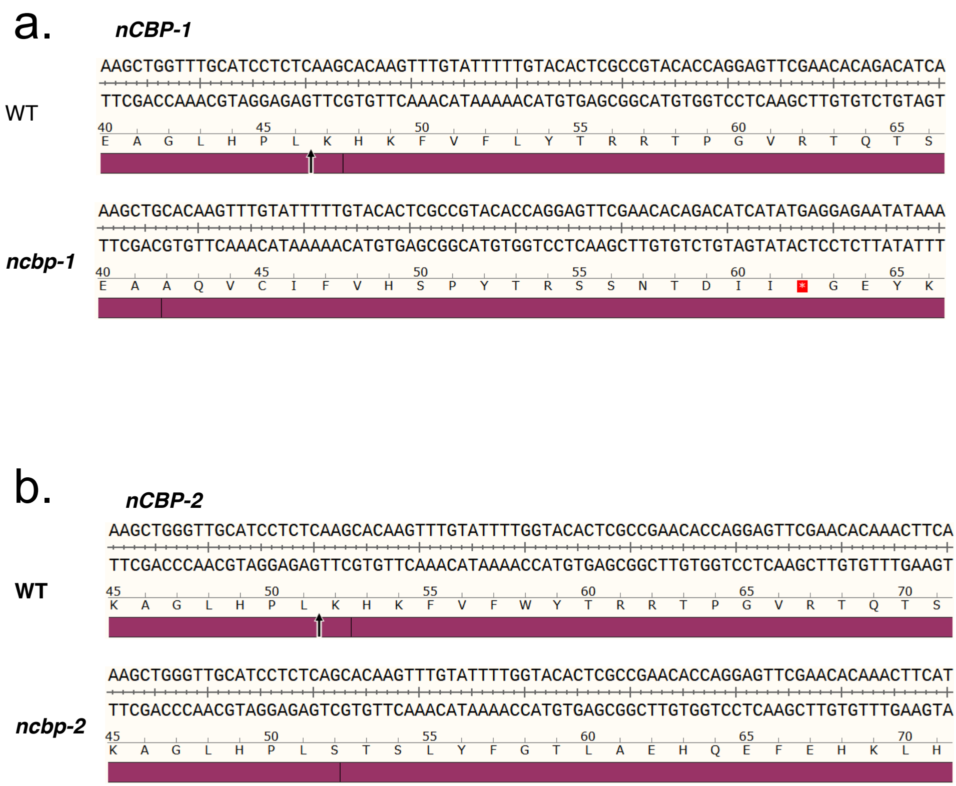

Figure S3. CRISPR/Cas9 –induced mutagenesis creates out of frame alternate splice variants. Exon 1 and exon 2 splice junction of *nCBP-1* (a) and *nCBP-2* (b) were examined via sequence analysis of cDNA. Predicted Cas9 cut site is shown as a black arrow. STOP codon is shown as starred, red box.

Target Gene	Construct	Line	Target Position	Mutation Zygosity	Genotype	Effect
nCBP-1	BS01	1	133	Homozygous	d3	Frameshift
		3	133	Chimeric	d4, i1, d1, d2	Frameshift, Frameshift, Frameshift, Frameshift
		4	133	Bi-allelic	d3, d9	Frameshift, Frameshift
		5	133	WT	WT	No effect
		6	133	Homozygous	i1	Frameshift
		7	133	Chimeric	d4, d1, d19, d34i16	Frameshift, Frameshift, Frameshift, Frameshift
	BS03	2	2677	WT	WT	No effect
		3	2677	Homozygous	d9	Frameshift
		4	2677	Bi-allelic	i3d2, i1	Frameshift, No effect
		5	2677	Homozygous	i1	No effect
		6	2677	Homozygous	d1	Frameshift
		7	2677	Bi-allelic	d3, i1	1 AA deleted and 1 AA changed, No effect
		8	2677	Bi-allelic	d12, i1	Frameshift, No effect
		9	2677	Homozygous	i1	No effect
		10	2677	Bi-allelic	d93i2, d2	Frameshift, Frameshift
		11	2677	Bi-allelic	d5, d1	Frameshift, Frameshift
nCBP-2	BS02	1	148	Chimeric	d3, d6, d7, i2d8	1 AA deletion and 1 AA changed, Frameshift, Frameshift, Frameshift
		2	148	Bi-allelic	d5, d2	Frameshift, Frameshift
		4	148	Bi-allelic	i4d127, i8d20	Frameshift, Frameshift
		5	148	Chimeric	d17, d52, d1, i2d4	Frameshift, Frameshift, Frameshift, Frameshift
		6	148	Homozygous	d1	Frameshift
		7	148	Bi-allelic	d1, d17	Frameshift, Frameshift
	BS04	1	2763	Heterozygous	WT, i1	No effect , Frameshift
		2	2763	Bi-allelic	i1, d7	Frameshift, Frameshift
		3	2763	Chimeric	i1, d7, d4	Frameshift, Frameshift, Frameshift
		4	2763	Bi-allelic	d4, i1	Frameshift, Frameshift
		5	2763	Bi-allelic	d2, d6	Frameshift, 2 AA deletion
		6	2763	WT	WT	No effect
		8	2763	Homozygous	i1	Frameshift
		9	2763	Bi-allelic	d2, d7	Frameshift, Frameshift
		10	2763	Bi-allelic	i1d8, d2	Frameshift, Frameshift
		11	2763	Bi-allelic	d2, i1d10	Frameshift, Frameshift
		12	2763	Bi-allelic	d5, d11	Frameshift, Frameshift
		13	2763	Homozygous	d2	Frameshift
		14	2763	Bi-allelic	d7, d2	Frameshift, Frameshift
		15	2763	Bi-allelic	i1, d2	Frameshift, Frameshift
		16	2763	Bi-allelic	i1, d5	Frameshift, Frameshift
nCBP-1/2	BS05	1	148	Bi-allelic	d7, d1	Frameshift, Frameshift
			133	Bi-allelic	d2, d4	Frameshift, Frameshift
		2	148	Homozygous	d11	Frameshift
			133	Homozygous	i1	Frameshift
		3	148	Bi-allelic	i1, d1	Frameshift, Frameshift
			133	Bi-allelic	d1, d5	Frameshift, Frameshift
		4	148	Bi-allelic	d5, d4	Frameshift, Frameshift
			133	Bi-allelic	d2, d1	Frameshift, Frameshift
		5	148	Bi-allelic	i1, d6	Frameshift, Frameshift
			133	Bi-allelic	d4, d9	Frameshift, Frameshift
		6	148	WT	WT	No effect
			133	WT	WT	No effect
		7	148	Bi-allelic	i1, d15	Frameshift, Frameshift
			133	Bi-allelic	d3, d5	Frameshift, Frameshift
		8	148	Homozygous	d1	Frameshift
			133	Bi-allelic	d3, d1	Frameshift, Frameshift
eIF4E	BS06	3	1892	Bi-allelic	d1, d7	Frameshift, Frameshift
		4	1892	Homozygous	i1	Frameshift
		5	1892	Bi-allelic	d3, d4	1 AA deletion, Frameshift
		6	1892	Bi-allelic	d3, d4	1 AA deletion, Frameshift
		7	1892	Homozygous	d2	Frameshift
		8	1892	Homozygous	i1	Frameshift
		11	1892	Bi-allelic	d3, d12	1 AA deletion, 4 AA deletion
	BS07	1	-16	WT	WT	No effect
		2	-16	Bi-allelic	d2i1, d15i12	Start codon removal, Start codon removal
		9	-16	Bi-allelic	d4, i1	No effect

Table S1. Genotypes of all transgenic T_0 cassava lines.
WT, wild-type alleles; bi-allelic, two different mutated alleles; heterozygous, wild-type and mutated alleles; chimeric, more than two mutated alleles. d# and i# refer to deletions and insertions, respectively, with the number of bases mutated denoted by #. Highlighted transgenic events were used in CBSV/UCBSV challenge assays.

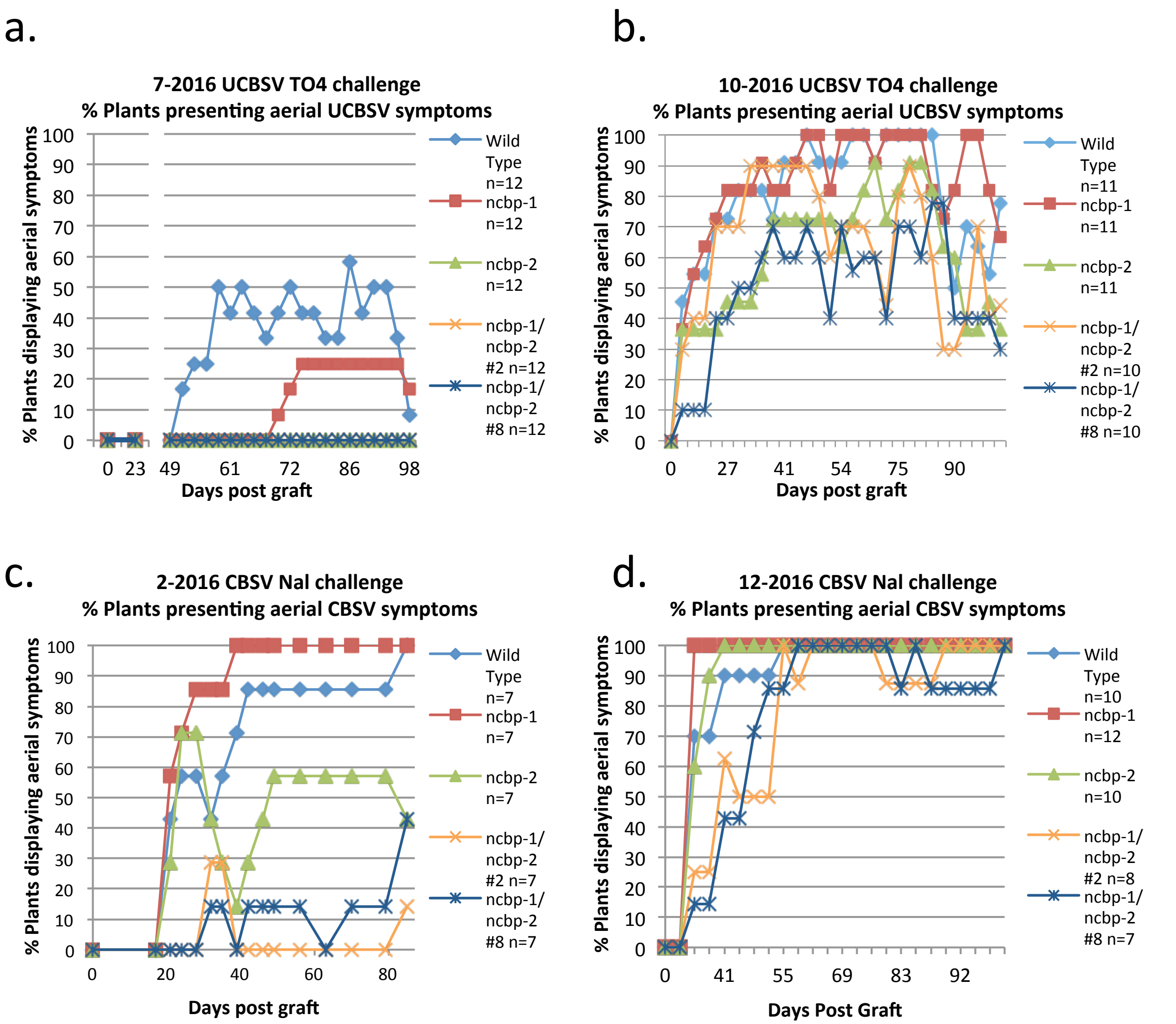

Figure S4. *ncbp-1 ncbp-2* double mutants exhibit reduced UCBSV symptom incidence and slowed CBSV symptom onset (a), (b), aerial symptom incidence reported as percent of wild type, *ncbp-1*, *ncbp-2*, or *ncbp-1 ncbp-2* plants bud-graft inoculated with UCBSV T04 (n≥10). (c), (d), aerial symptom incidence as previously described in plants inoculated with CBSV Naliendele (n≥7).

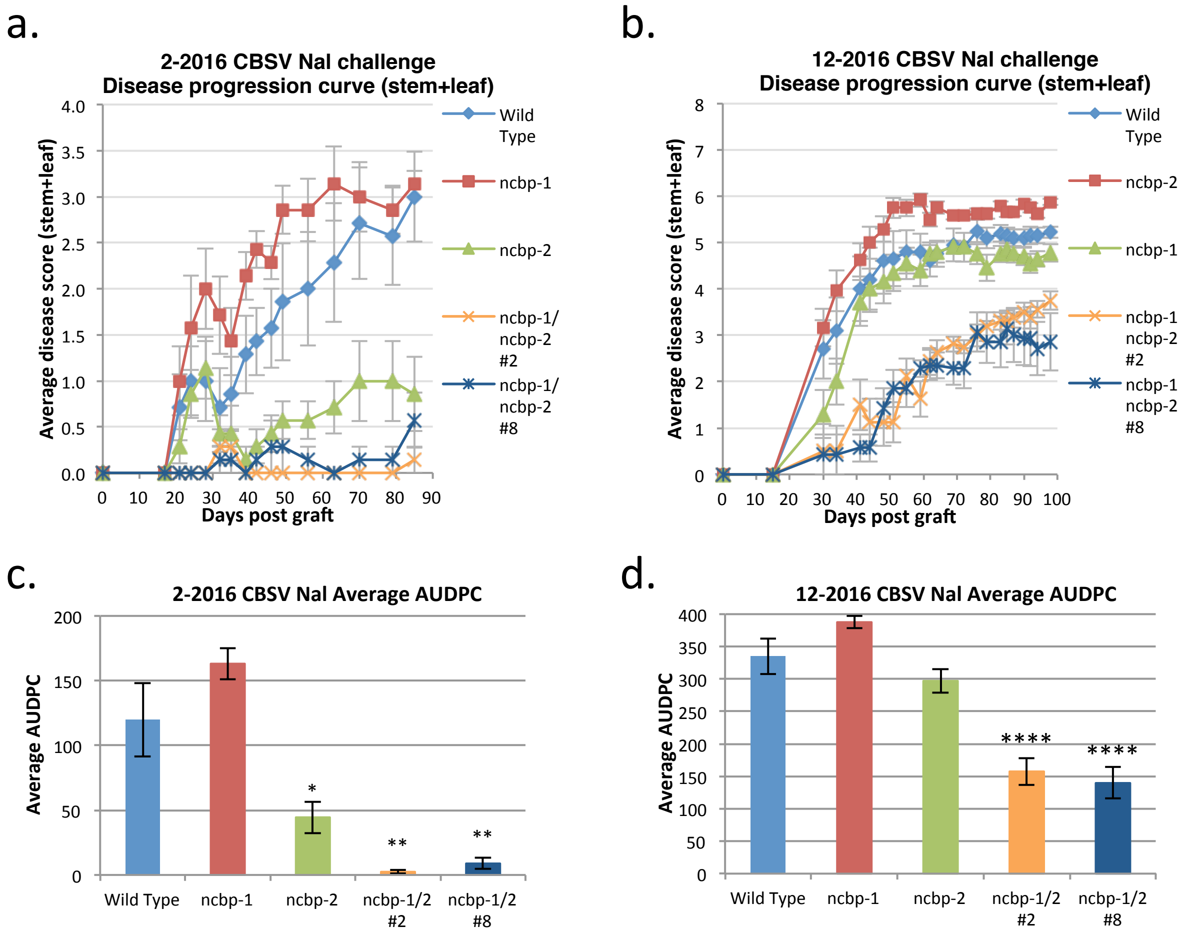

Figure S5. *ncbp-1 ncbp-2* double mutants exhibit reduced aerial CBSV symptom severity
(a), (b), disease progression curves of wild type, *ncbp-1*, *ncbp-2*, or *ncbp-1 ncbp-2* plants bud-graft inoculated with CBSV Naliendele (n≥7). Leaf and stem symptoms were each scored on a 0-4 scale and summed to obtain an aggregate aerial score. (c), (d), average area under the disease progression curve (AUDPC) derived from data plotted in (a) and (b). Error bars indicate standard error of the mean. Statistical differences were detected by Welch's t-test, α=0.05, *≤0.05, **≤0.01, ****≤0.0001.

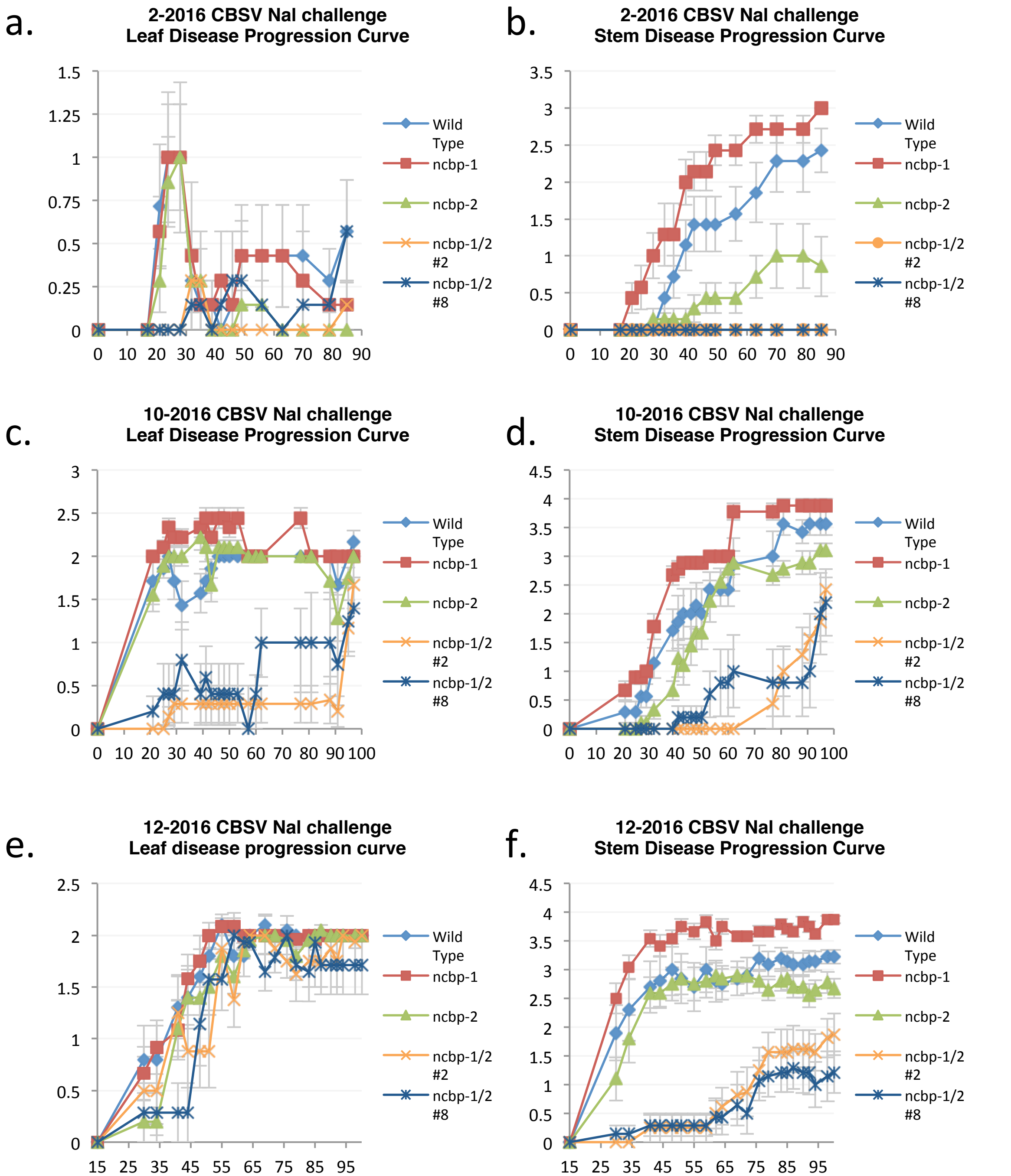

Figure S6. *ncbp-1/ncbp-2* stem symptom severity is consistently reduced across all experiments
Separate leaf and stem disease progression curves for wild type, *ncbp-1*, *ncbp-2*, or *ncbp-1 ncbp-2* plants bud-graft inoculated with CBSV Naliendele (n≥7). Leaf and stem symptoms were each scored on a 0-4 scale. (a), (c), and (e) represent leaf disease progression curves from three different experiments while (b), (d), and (f) represent corresponding stem disease progression curves. Error bars represent standard error of the mean.

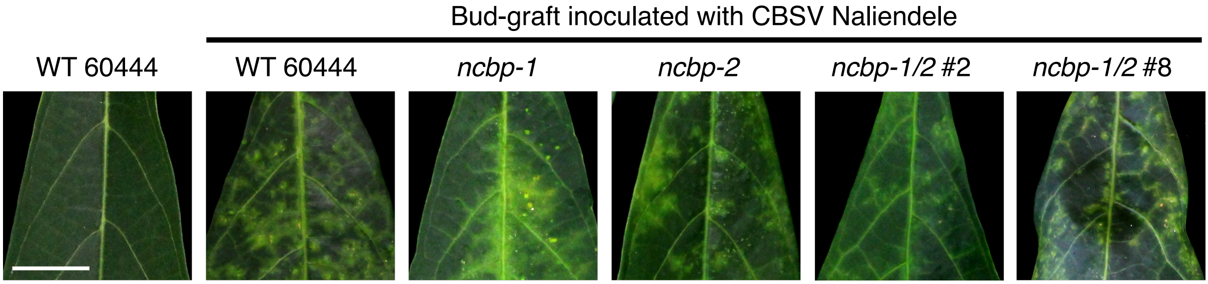

Figure S7. 12-2016 CBSV challenge leaf symptom severity is similar across all genotypes
Wild type, *ncbp-1*, *ncbp-2*, or *ncbp-1 ncbp-2* plants bud-graft inoculated with CBSV Naliendele isolate all develop widespread chlorotic leaf symptoms. Leaf images were taken near 12-2016 challenge endpoint. Scale bar denotes one centimeter.

Tissue specific expression of cassava *eIF4E* isoforms

Gene	FEC	Fibrous Root	Lateral Bud	Leaf	Mid Vein	OES	Petiole	RAM	SAM	Stem	Storage root
eIF(iso)4E-1	51	28	19	15	12	42	20	70	36	26	28
eIF(iso)4E-2	85	65	49	72	48	81	67	148	74	73	73
nCBP-2	154	185	362	96	113	597	105	142	165	121	1259
nCBP-1	15	51	23	117	91	11	121	38	18	71	114
eIF4E	72	94	74	69	61	72	82	210	104	89	87

shiny.danforthcenter.org/cassava_atlas/

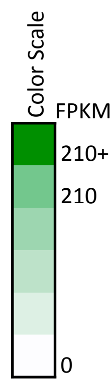

Figure S8. *nCBP-1* is highly expressed in storage roots
Heat map describing tissue specific expression of cassava *eIF4E* isoforms. Data was extracted from the Bart Lab Cassava Atlas (http://shiny.danforthcenter.org/cassava_atlas/). Expression values are defined as fragments per kilobase of transcript per million mapped reads (FPKM).

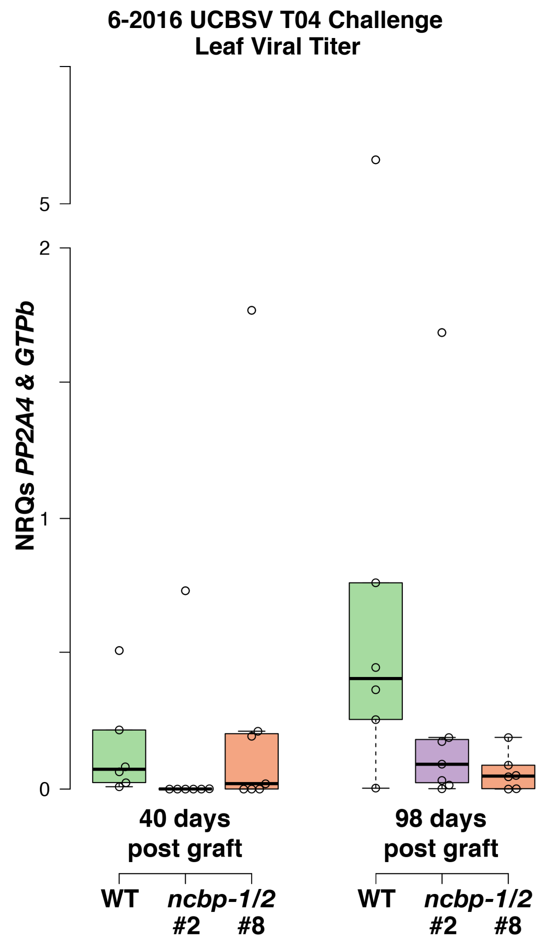

Fig S9. 6-2016 UCBSV challenge virus titer analysis
Quantitative real time PCR analysis of UCBSV T04 titer in wild type, *ncbp-1/2* #2, and *ncbp-1/2* #8 leaf tissue. Leaf samples were collected from the first fully expanded leaf at each time-point. n≥6 per genotype. Whiskers span the interquartile range, solid bars indicate the median of scores.